JBC RESEARCH ARTICLE

# Inhibition of high-fat diet–induced obesity *via* reduction of ER-resident protein Nogo occurs through multiple mechanisms

Received for publication, July 21, 2021, and in revised form, December 18, 2021 Published, Papers in Press, January 5, 2022,
https://doi.org/10.1016/j.jbc.2022.101561

**Xiaolin Wang[1], Yanfang Yang[1], Dan Zhao[1], Shuang Zhang[2], Yi Chen[1], Yuanli Chen[2], Ke Feng[1], Xiaoju Li[1], Jihong Han[1,2], Yasuko Iwakiri[3], Yajun Duan[2,*], and Xiaoxiao Yang[2,*]**

*From the [1]State Key Laboratory of Medicinal Chemical Biology, Key Laboratory of Bioactive Materials of Ministry of Education, College of Life Sciences, Nankai University, Tianjin, China; [2]Key Laboratory of Metabolism and Regulation for Major Diseases of Anhui Higher Education Institutes, College of Food and Biological Engineering, Hefei University of Technology, Hefei, China; [3]Section of Digestive Diseases, Yale University School of Medicine, New Haven, Connecticut, USA*

Edited by Qi Qun Tang

**Obesity is a risk factor for insulin resistance, type 2 diabetes, and cardiovascular diseases. Reticulon-4 (Nogo) is an endoplasmic reticulum–resident protein with unclear functions in obesity. Herein, we investigated the effect of Nogo on obesity and associated metabolic disorders. Human serum samples were collected to explore the relationship between circulating Nogo-B and body mass index value. Nogo-deficient and WT littermate control mice were fed normal chow or high-fat diet (HFD) for 14 weeks, and HFD-induced obese C57BL/6J mice were injected scrambled or Nogo siRNA for 2 weeks. We found that in human and mouse serum, Nogo-B was positively correlated to body mass index/bodyweight and lipid profiles. Reduced Nogo (by genetic deletion or siRNA transfection) protected mice against HFD-induced obesity and related metabolic disorders. We demonstrate that Nogo deficiency reversed HFD-induced whitening of brown adipose tissue, thereby increasing thermogenesis. It also ameliorated lipid accumulation in tissues by activating the adiponectin–adiponectin receptor 1–AMP-activated kinase α signaling axis. Finally, Nogo deficiency potently reduced HFD-induced serum proinflammatory cytokines and infiltration of macrophages into metabolic organs, which is related to enhanced NF-κB p65 degradation *via* the lysosome pathway. Collectively, our study suggests that reduced levels of Nogo protect mice against HFD-induced obesity by increasing thermogenesis and energy metabolism while inhibiting NF-κB-mediated inflammation. Our results indicate that inhibition of Nogo may be a potential strategy for obesity treatment.**

Obesity has become a public health issue that impairs the quality of life, raises health care costs, and increases the risk of health complications, including insulin resistance, type 2 diabetes, and cardiovascular diseases. The prevalence of obesity was 10.8% in men and 14.9% in women in 2014 and will increase to 18% and 21% by 2025 (1). The rising obesity prevalence calls for effective strategies for prevention and/or treatment. Several approved drugs, such as lorcaserin, phentermine, and liraglutide, are not effective enough while having severe side effects (2). Therefore, exploring effective and safe strategies for obesity treatment is still an urgent need.

Obesity can cause chronic low-grade inflammation in multiple organs, including adipose tissue, liver, skeletal muscle, and pancreatic islets (3–5). In turn, the inflammation in these tissues can aggravate obesity and obesity-associated complications, leading to vicious cycles. NF-κB is a key transcription factor controlling inflammatory process. NF-κB family consists of RelA/p65, RelB, c-Rel, p50/NF-κB1, and p52/NF-κB2 in mammals. They bind to target DNA as homodimers or heterodimers, of which the p65 and p50 heterodimers is the most common one (6). In physiological state, NF-κB locates in cytoplasm inactively. Once stimulated, it can translocate into nucleus and trigger the transcription of target genes including interlukin-1 (IL-1), IL-6, and interferon-γ (7). NF-κB is deeply involved in the development of obesity and its complications (7). Deficiency of NF-κB p50 protects mice against high-fat diet (HFD)-induced obesity, insulin resistance, and liver steatosis (8). Liver-specific NF-κB p65 deletion ameliorates HFD-impaired insulin sensitivity (9). IL-1β, a target of NF-κB, is highly associated with human body mass index (BMI) and fasting blood glucose levels (10). Inactivation of IL-1β protects mice against HFD-induced glucose tolerance and improves insulin secretion in type 2 diabetes patients (11, 12).

Reticulon-4 (Nogo) family consists of several members, including Nogo-A, Nogo-B, and Nogo-C. The expression of Nogo family members is in a tissue-dependent manner. Nogo-A is mainly expressed in central nervous system, whereas Nogo-B is widely expressed in various tissues (13). Nogo-B is the only member detectable in liver and circulation (14). Several biological functions of Nogo have been reported. For instance, it influences ischemic injury and alcoholic liver disease by regulating macrophage infiltration and Kupffer cell polarization in mice (15, 16). Recently, we reported that reduced Nogo expression protected mice against high-carbohydrate diet–induced hepatic steatosis and insulin

* For correspondence: Xiaoxiao Yang, yangxiaoxiao@hfut.edu.cn; Yajun Duan, yduan@hfut.edu.cn.

resistance by regulating carbohydrate-responsive element–binding protein and insulin activity (14). These studies imply that Nogo can play an important role in different types of metabolic disorders. Obesity is contributed by different factors, such as chronic inflammation, imbalance between energy intake, and expenditure. Thus, we investigated if inhibited Nogo expression can reduce HFD-induced obesity by multiple mechanisms.

## Results

### *Human serum Nogo-B is correlated with BMI and lipid profiles, and mouse tissue Nogo-B expression is activated by dietary lipid supplement*

Serum samples were collected from volunteers with different BMI values: underweight (BMI <18.5 kg/m$^2$), normal (18.5 kg/m$^2$ ≤ BMI <24 kg/m$^2$), overweight (24 kg/m$^2$ ≤ BMI <28 kg/m$^2$), and obese (BMI ≥ 28 kg/m$^2$), according to the obesity definition in China (17). We then determined levels of Nogo-B and lipid profiles (triglyceride [TG], total cholesterol [T-CHO], and low-density lipoprotein cholesterol [LDL]) in human serum samples. As shown in Figure 1*A*, serum Nogo-B levels increased along with BMI increment. Furthermore, the correlation assay suggests that serum Nogo-B levels are positively correlated to BMI ($R$ = 0.405; $p$ = 0.004), TG ($R$ = 0.321; $p$ = 0.023), T-CHO ($R$ = 0.315; $p$ = 0.026), and LDL ($R$ = 0.281; $p$ = 0.049) (Fig. 1, *B* and *C*), indicating that circulating Nogo-B might be associated with development of obesity and its complications.

To determine if tissue Nogo-B expression can be regulated by different dietary conditions, mice were fasted for 24 h and then refed normal chow for 12 h. Figure 1*D* shows that Nogo-B expression in liver, epididymal white adipose tissue (eWAT), and skeletal muscle was all increased by refeeding. Feeding mice an HFD (35% fat) or a high-cholesterol diet (21% fat plus 0.5% cholesterol) for 1 week also substantially upregulated Nogo-B expression in these tissues (Fig. 1, *E* and *F*). Thus, Nogo-B in circulation or tissues with high metabolic activity are increased with obesity or food containing high lipids.

### *Nogo deficiency ameliorates HFD-induced obesity*

In mice, Nogo-A is mainly expressed in brain. Nogo-B is detectable in various tissues (Fig. S1, *A* and *B*). The high homology among Nogo family members indicates it is impossible to generate Nogo-B global-deficient mice (14). Therefore, we used Nogo-deficient (Nogo$^{-/-}$ or Nogo KO) mice to investigate the pathophysiological functions of Nogo-B on HFD-induced obesity. Both Nogo$^{-/-}$ and littermate control (WT or Ctrl) mice were fed normal chow or HFD for 14 weeks.

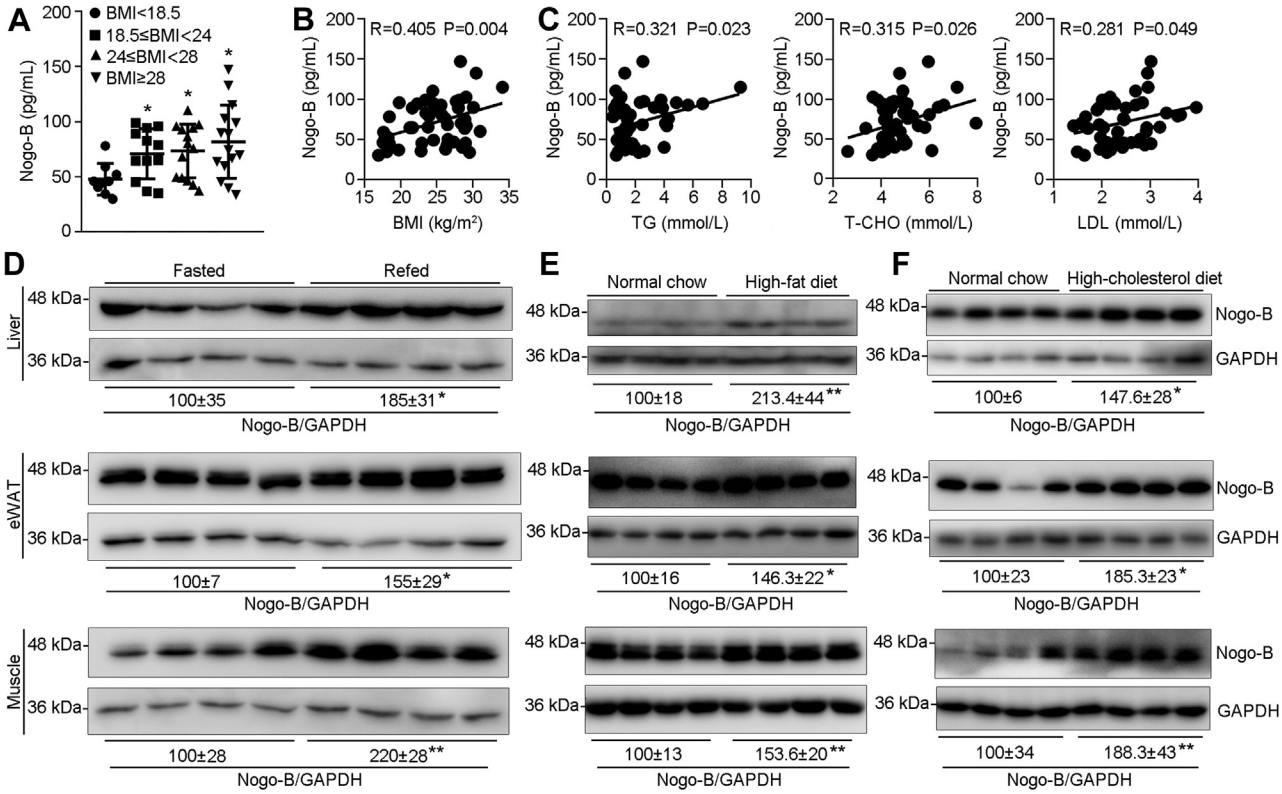


**Figure 1. Activated Nogo-B is associated with obesity and overnutrition conditions.** Serum samples collected from volunteers (n = 50) were determined levels of Nogo-B, TG, T-CHO, and LDL. *A*, Nogo-B levels were grouped based on the BMI ranges (BMI < 18.5 kg/m$^2$, n = 9; 18.5 kg/m$^2$ ≤ BMI < 24 kg/m$^2$, n = 12; 24 kg/m$^2$ ≤ BMI < 28 kg/m$^2$, n = 14; BMI ≥ 28 kg/m$^2$, n = 15). The correlation coefficient between Nogo-B and BMI (*B*) or lipid profiles (TG, T-CHO, and LDL) (*C*) in humans was analyzed using the Pearson correlation test with 95% confidence interval. Male C57BL/6J mice (~7 weeks old) were used to conduct fasting (*D*), 1 week HFD (*E*), or high-cholesterol diet (*F*) feeding, followed by determination of Nogo-B expression by Western blot with total proteins extracted from liver, eWAT, and skeletal muscle samples. *$p$ < 0.05 and **$p$ < 0.01 (n = 4). BMI, body mass index; eWAT, epididymal white adipose tissue; HFD, high-fat diet; LDL, low-density lipoprotein cholesterol; Nogo, reticulon-4; T-CHO, total cholesterol; TG, triglyceride.

Compared with normal chow, HFD feeding substantially increased bodyweight in both littermate Ctrl and Nogo$^{-/-}$ mice. However, bodyweight gain was much less in Nogo$^{-/-}$ than WT mice, particularly by HFD (Fig. 2, *A* and *B*), indicating that Nogo deficiency inhibits HFD-induced obesity. No difference of food intake or excretion of TG and T-CHO in feces between two groups was determined, which confirms that the reduced bodyweight gain in Nogo$^{-/-}$ mice is not

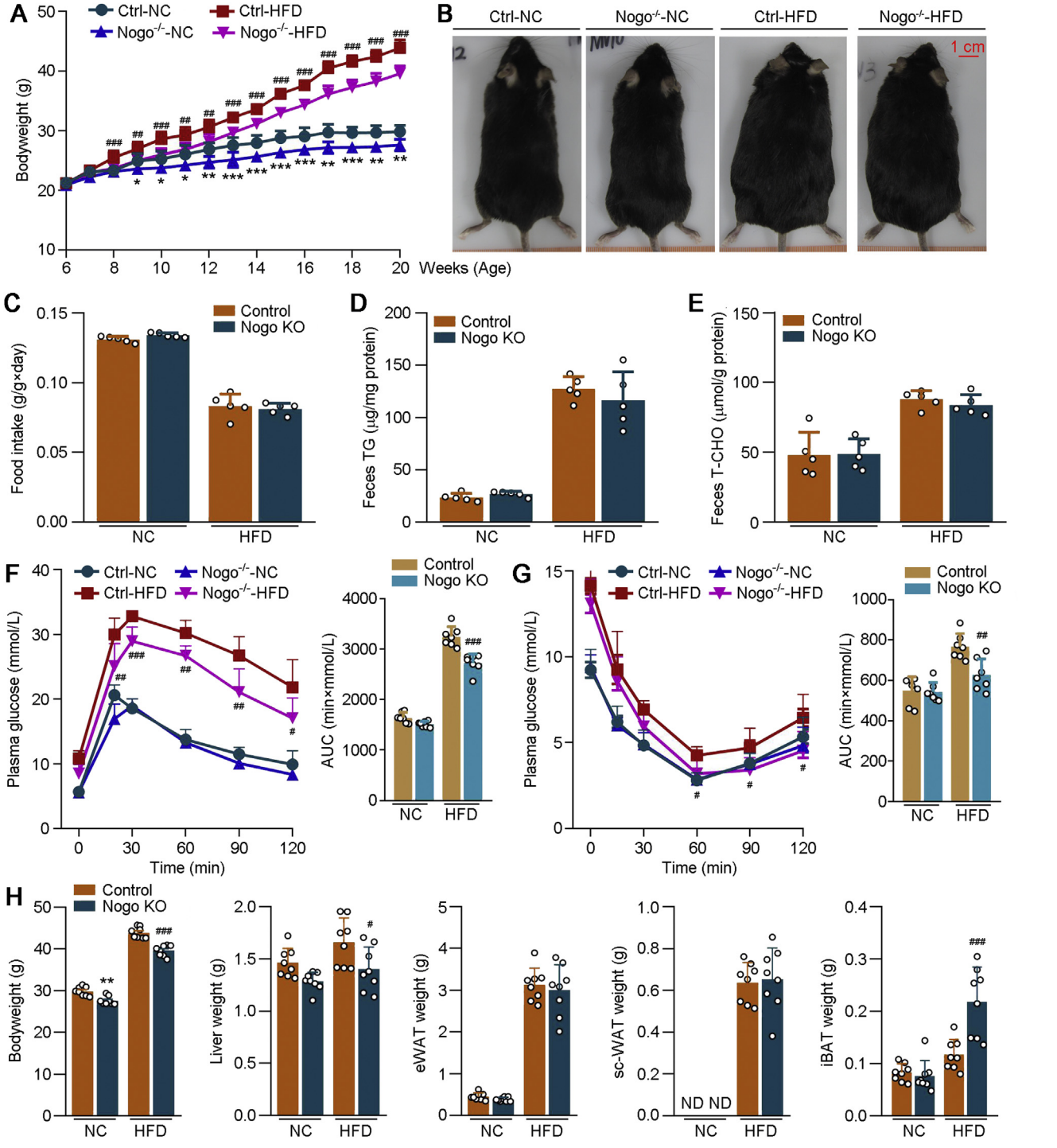


**Figure 2. Nogo deficiency ameliorates HFD-induced obesity, glucose intolerance, and insulin resistance.** Nogo-deficient (Nogo KO, Nogo$^{-/-}$) and littermate control mice (Control or Ctrl) (males, ~6 weeks old) were fed normal chow (NC) or HFD for 14 weeks. *A*, during the treatment, mouse bodyweight was determined weekly. *B* and *H*, at the end of experiment, mice were photographed; bodyweight and weight of the collected tissues (liver, eWAT, sc-WAT, and iBAT) were determined (n = 8). During the experiment (~15 weeks old or the ninth week of experiment), food consumption (*C*), triglyceride (*D*), and T-CHO (*E*) in feces were determined (n = 5). *F* and *G*, GTT or ITT was conduced on the mice at the 12th or 13th week of the experiment (n = 8). $^{*}p < 0.05$, $^{**}p < 0.01$, $^{***}p < 0.001$ *versus* control NC-fed mice; $^{\#}p < 0.05$, $^{\#\#}p < 0.01$, $^{\#\#\#}p < 0.001$ *versus* control HFD-fed mice. AUC, area under curve; eWAT, epididymal white adipose tissue; GTT, glucose tolerance test; HFD, high-fat diet; iBAT, interscapular brown adipose tissue; ITT, insulin tolerance test; ND, under detectable; Nogo, reticulon-4; sc-WAT, subcutaneous white adipose tissue; T-CHO, total cholesterol.

because of food consumption or absorption (Fig. 2, *C–E*). Using indirect calorimetry, we found that Nogo deficiency significantly increased body oxygen consumption and energy expenditure, whereas it had little effect on mice physical activity under HFD condition (Fig. S2). Collectively, aforementioned results indicate that Nogo deficiency ameliorates HFD-induced obesity by enhancing energy metabolism.

Table S1 shows that Nogo deficiency significantly reduced postprandial hyperglycemia regardless of food types. Correspondingly, the obesity-induced glucose intolerance and insulin resistance were markedly ameliorated in Nogo$^{-/-}$ mice (Fig. 2, *F* and *G*), indicating that Nogo deficiency greatly improves HFD-impaired blood glucose homeostasis and insulin sensitivity.

Nogo deficiency decreased mouse liver weight, whereas substantially increased interscapular brown adipose tissue (iBAT) weight under HFD feeding (Fig. 2*H*). Therefore, Nogo deficiency inhibits HFD-induced obesity and ameliorates obesity-associated indicators.

### *Nogo deficiency promotes healthy expansion of adipose tissue*

Under the overnutrition, adipose tissue can expand rapidly to maintain nutrient homeostasis. HFD enlarged adipocytes in both WT and Nogo$^{-/-}$ mice with reduced effect on Nogo$^{-/-}$ mice (Fig. 3, *A* and *B*), indicating less lipid accumulation in eWAT of Nogo$^{-/-}$ mice. Adiponectin, an important adipokine secreted by adipose tissue, can improve insulin sensitivity and energy metabolism by activating AMP-activated kinase α (AMPKα) (18). Leptin, another major adipokine, is positively correlated to the bodyweight. Nogo$^{-/-}$ mice showed elevated adiponectin mRNA expression associated with increased circulating high–molecular weight (HMW) adiponectin (Figs. 3*C* and S3*A*). Nogo deficiency also reduced leptin mRNA level in eWAT under HFD condition (Fig. 3*D*).

Adipose tissue expansion is not always accompanied by detrimental pathological changes. For instance, that featured by enhanced angiogenesis and reduced fibrosis is regarded as a healthy adipose tissue expansion (19, 20). Interestingly, Nogo deficiency activated expression of vascular endothelial growth factor β (Vegf-β), an angiogenesis-related gene, in HFD-fed mouse eWAT (Fig. 3*E*). Collagen VI is the main form of collagen produced by adipocytes (21). Nogo deficiency reduced HFD-activated collagen type VI α2 expression in eWAT (Fig. 3*F*). Correspondingly, the results of Sirius red staining further confirm reduced fibrosis in eWAT of Nogo$^{-/-}$ mice (Fig. 3*G*). Similarly, reduced adipocyte size, leptin, collagen type VI α1, and increased adiponectin and Vegf-β, were determined in the subcutaneous white adipose tissue (sc-WAT) of HFD-fed Nogo$^{-/-}$ mice (Fig. 3, *H–N*). Therefore, a healthy expansion occurs to Nogo$^{-/-}$ mouse adipose tissues under HFD feeding.

To investigate the regulation of Nogo on aforementioned phenotypes, we first detected Nogo protein expression in adipocytes and stromal vascular fraction (SVF) from eWAT. As shown in Fig. S4*A*, Nogo protein levels in adipocytes and SVF were comparable and can be induced by HFD. Then, we constructed Nogo-deficient 3T3-L1 cells and found that Nogo deficiency attenuated palmitate-reduced adiponectin mRNA levels, whereas had little effect on Vegf-β mRNA expression in 3T3-L1–derived adipocytes (Fig. S4, *B–D*). In addition, the induction of transforming growth factor beta on collagen type VI α1 and collagen type VI α2 mRNA expression was ameliorated by Nogo deficiency (Fig. S4, *E* and *F*). Taken together, the effects of Nogo deficiency on adiponectin and collagen type VI α1 or α2 expression are partially dependent on the direct deficiency of Nogo in adipocytes.

### *Nogo deficiency enhances browning of adipose tissue*

BAT, a metabolically active tissue, supports energy metabolism by converting lipids into heat. The high expression of Nogo-B in iBAT indicates that BAT may be a critical tissue affected by Nogo deficiency (Fig. S1*A*). HFD increased iBAT weight moderately in WT mice (∼45%) but potently in Nogo$^{-/-}$ mice (∼190%) (Fig. 2*H*). The increase of iBAT weight can be due to the browning of adipocytes and/or enlarged adipocyte size by lipid accumulation. The H&E staining of iBAT sections demonstrates that HFD increased iBAT adipocyte size in both WT (∼120%) and Nogo$^{-/-}$ mice (∼80%), indicating lipid accumulation occurred to cells. However, the average adipocyte size in HFD-fed Nogo$^{-/-}$ mice was smaller than that in WT mice (Fig. 4*A*), suggesting that more brown adipocytes are conserved, or obesity-induced iBAT whitening is reversed in HFD-fed mice by Nogo deficiency. Consistently, mRNA levels of brown adipocyte markers (uncoupling protein-1 [Ucp-1]; T-box transcription factor 1; and cell death–inducing DNA fragmentation factor-alpha–like effector α) were upregulated in HFD-fed Nogo$^{-/-}$ mice (Fig. 4*B*). HFD-decreased UCP-1 expression was partially restored by Nogo deficiency (Fig. 4, *C* and *D*).

BAT stores lipid mainly in TG form and consumes fatty acids as thermogenic substrates (22). Therefore, we evaluated expression of TG hydrolysis–related genes (hormone-sensitive lipase and adipose TG lipase) and fatty acid oxidation–related genes (carnitine palmitoyltransferase 1β; cytochrome C oxidase subunit 5b and 8b; and NADH:ubiquinone oxidoreductase subunit b2) in the tissue and observed that these genes were all notably upregulated in HFD-fed Nogo$^{-/-}$ mice (Fig. 4, *E* and *F*).

To further confirm the role of Nogo in adipocyte browning and thermogenesis, we performed the cold adaptation experiment, in which both WT and Nogo$^{-/-}$ mice were housed in 24 h cycles of 12 h at 4 °C and another 12 h at room temperature for 1 week. Compared with mice under room temperature (Fig. S1*A*), Nogo-B protein levels were much lower in iBAT and sc-WAT than eWAT under cold exposure condition (Fig. S5*A*), further indicating the involvement of Nogo in thermogenesis. After cold exposure, Nogo deficiency increased mouse body temperature, weight of iBAT and sc-WAT, and multilocular beige cells in sc-WAT (Fig. 4, *H–J*). In addition, it increased UCP-1 expression in sc-WAT and iBAT and expression of PR domain containing 16 and deiodonase 2 mRNA (two BAT markers) in iBAT (Fig. 4, *K* and *M–O*). Thus, Nogo deficiency can promote adipose tissue browning and thermogenesis.

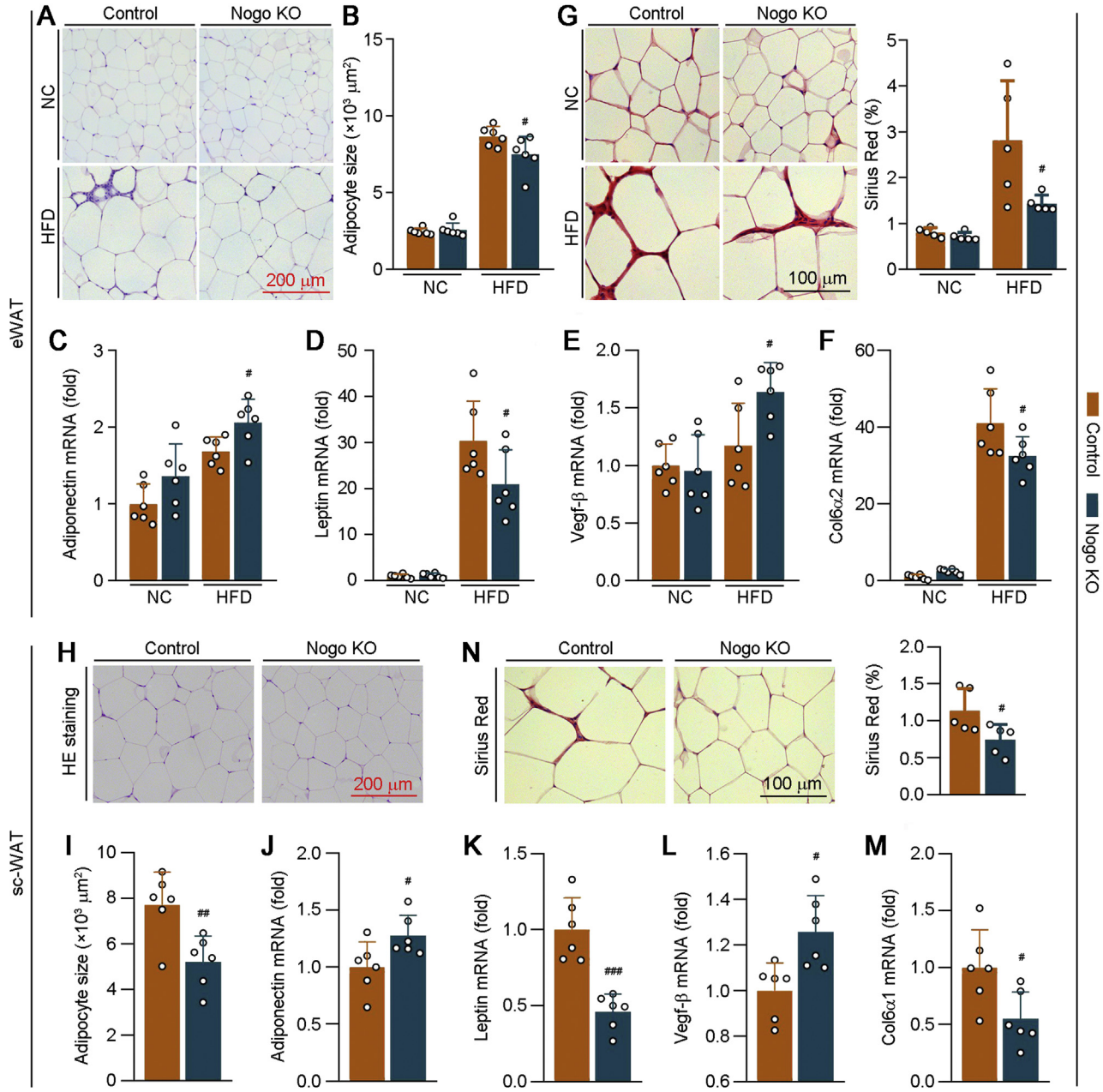


**Figure 3. Lack of Nogo expression promotes healthy expansion of adipose tissue by inhibiting fibrosis and collagen synthesis.** The following assays were conducted for eWAT and sc-WAT tissues collected from mice used in Figure 2. eWAT sections were conducted H&E staining (*A*) with quantitation of adipocyte size (*B*, n = 6) and Sirius red staining (*G*, n = 5). *C–F*, expression of adiponectin, leptin, Vegf-β, and Col6α2 mRNA in eWAT was determined by qRT–PCR (n = 6). sc-WAT sections of HFD-fed littermate control and Nogo$^{-/-}$ mice (it is hardly to collect sc-WAT when the animals were fed normal chow, Fig. 2*H*) were conducted H&E staining (*H*) with quantitation of adipocyte size (*I*, n = 6) and Sirius red staining (*N*, n = 5). *J–M*, expression of adiponectin, leptin, Vegf-β, and Col6α1 mRNA in sc-WAT was determined by qRT–PCR (n = 6). $^{\#}p < 0.05$, $^{\#\#}p < 0.01$, $^{\#\#\#}p < 0.001$ *versus* control HFD-fed mice. Col6α1, collagen type VI α1; Col6α2, collagen type VI α2; eWAT, epididymal white adipose tissue; HFD, high-fat diet; NC, normal chow; Nogo, reticulon-4; qRT, quantitative RT; sc-WAT, subcutaneous white adipose tissue; Vegf-β, vascular endothelial growth factor β.

To determine whether Nogo regulates thermogenesis in a cell autonomous mechanism, we first detected Nogo protein levels in adipocytes and SVF from iBAT. As shown in Fig. S5*B*, Nogo-B protein expression was much higher in adipocytes than SVF. *In vitro*, we transfected C3H10T1/2 cell-derived brown adipocytes with Nogo siRNA or Nogo expression vector, followed by isoproterenol treatment (a β-adrenoreceptor agonist that can stimulate thermogenesis). The results in Fig. S5, *C* and *D* showed that Nogo knockdown increased UCP-1 expression, whereas Nogo overexpression reduced UCP-1 protein levels. Thus, Nogo regulates thermogenesis in a cell-autonomous manner, at least partly.

### *Nogo deficiency protects mice against HFD-induced lipid accumulation in liver and skeletal muscle*

The reduced liver weight in HFD-fed Nogo$^{-/-}$ mice (Fig. 2*H*) implies that Nogo deficiency may inhibit obesity-

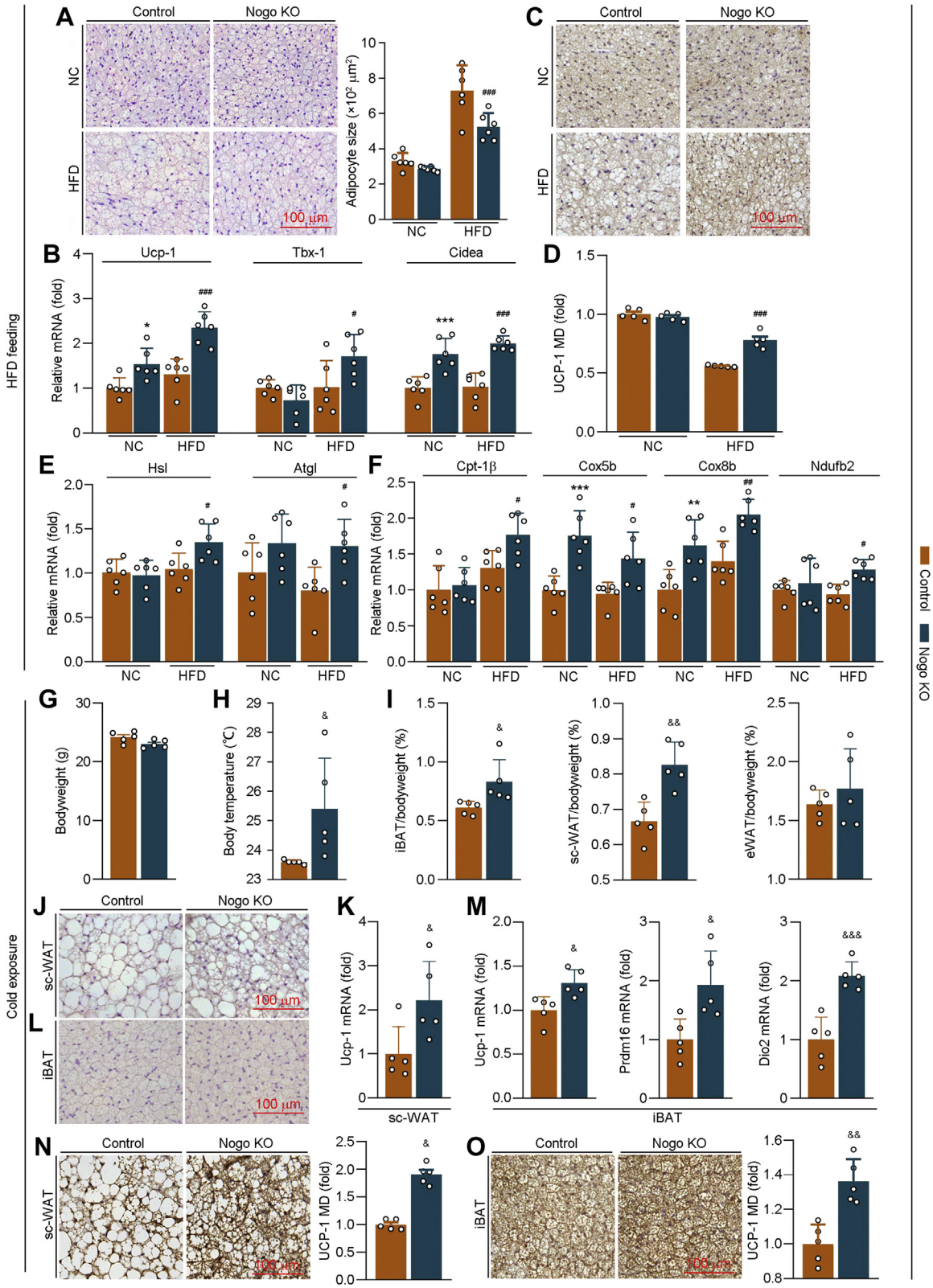


**Figure 4. Nogo deficiency enhances browning of adipose tissue in HFD feeding or cold exposure situation by promoting expression of thermogenic genes.** At the end of experiment as indicated in Figure 2, iBAT was collected, and the tissue sections were conducted H&E staining with quantitation of adipocyte size (*A*, n = 6) and UCP-1 immunohistochemical staining (*C*) with quantitation of mean density (MD) (*D*, n = 5). Expression of thermogenic genes (Ucp-1, Tbx-1, and Cidea; *B*), TG hydrolysis–related genes (Hsl and Atgl; *E*), and fatty acid oxidation–related genes (Cpt-1β, Cox5b, Cox8b, and Ndufb2; *F*) were determined by qRT–PCR (n = 6). $^{*}p < 0.05$, $^{**}p < 0.01$, $^{***}p < 0.001$ *versus* control NC-fed mice; $^{\#}p < 0.05$, $^{\#\#}p < 0.01$, $^{\#\#\#}p < 0.001$ *versus* control HFD-fed mice. Male littermate control and Nogo$^{-/-}$ mice (∼10 weeks old, five mice per group) were housed at the 24 h cycles of 12 h at 4 °C and 12 h at room temperature for 7 days. At the end of experiment, bodyweight (*G*) and body temperature (*H*) were measured. iBAT, sc-WAT, and eWAT were collected, weighed, and calculated as percent of tissue weight in bodyweight (*I*). sc-WAT and iBAT sections were conducted H&E staining (*J* and *L*) and

induced hepatic steatosis. Indeed, both H&E and Oil red O staining demonstrate that Nogo deficiency substantially blocked HFD-increased hepatic lipid accumulation, evidenced by fewer vacuoles in H&E staining and lighter Oil red O staining (Fig. 5*A*). Consistently, Nogo deficiency reduced HFD-increased TG and free fatty acid (FFA) levels in the liver (Fig. 5, *B* and *C*). It also reduced circulating TG (Table S1), whereas had little effect on liver T-CHO levels (Fig. 5*D*).

Although mRNA expression of TG synthesis (diacylglycerol O-acyltransferase), fatty acid uptake–related genes (fatty acid–binding protein 1 and 4), or synthesis-related genes (acetyl-CoA carboxylase α and stearoyl-CoA desaturase-1 [Scd1]), or protein expression of fatty acid synthase and SCD was not influenced by Nogo deficiency (Figs. 5*E* and S6), mRNA expression of TG hydrolysis–related genes (hormone-sensitive lipase and adipose TG lipase) and fatty acid oxidation–related genes (acyl-CoA oxidase 1 and 2; peroxisome proliferator–activated receptor [PPAR] gamma coactivator 1α [Pgc-1α]; and carnitine palmitoyltransferase 1α) was markedly upregulated in HFD-fed Nogo$^{-/-}$ mice (Fig. 5, *E* and *F*), suggesting that ameliorated HFD-induced hepatic lipid accumulation by Nogo deficiency is related to activation of TG hydrolysis and fatty acid oxidation or energy metabolism.

AMPKα is a pivotal regulator in energy metabolism, and activated AMPKα (phosphorylated AMPKα [p-AMPKα]) can increase lipid oxidation. In agreement with the aforementioned results, p-AMPKα was significantly increased in Nogo$^{-/-}$ mouse liver (Fig. 5*G*). Circulating adiponectin can activate AMPKα by binding to adiponectin receptor 1 (AdipoR1) (23). Nogo deficiency increased AdipoR1 expression and serum HMW adiponectin in HFD-fed mice (Figs. 5, *G* and *H* and S3*A*). Therefore, much higher p-AMPKα was observed in Nogo$^{-/-}$ mice than WT mice at HFD feeding.

Consistent with the results in *in vivo* study, protein levels of AdipoR1 and p-AMPKα in Nogo-deficient HepG2 (Nogo-Cas9) cells were also higher than Ctrl-Cas9 HepG2 cells, and the activation of AMPKα by AdipoRon (AdipoR1 agonist) was abolished in Nogo-Cas9 cells by AdipoR1 siRNA (Fig. S3, *B* and *C*), indicating that Nogo deficiency promotes adiponectin-induced p-AMPKα in an AdipoR1-dependent manner. Nogo deficiency also restored HFD-reduced PGC-1α and phosphorylated AKT (p-AKT) protein in mouse liver (Fig. 5*G*). These data suggest that Nogo deficiency promotes lipid oxidation through adiponectin–AdipoR1–AMPKα pathway, thereby improving obesity-induced metabolic disorders in the liver.

Obesity also elevates blood lipid levels and enhances lipid uptake in adipose tissue and skeletal muscle. The excess ectopic lipid accumulation in skeletal muscle can influence tissue functions (24). Similar to the liver (Fig. 5*B*), Nogo deficiency also reduced HFD-induced TG accumulation in skeletal muscle (Fig. 5*I*). PGC-1α is a key regulator of energy metabolism and mitochondrial biogenesis (25). Nuclear respiratory factor 1 is a main target of PGC-1α in this process. Compared with WT mice, Nogo deficiency activated PGC-1α protein expression (Fig. 5*J*). mRNA levels of nuclear respiratory factor 1 and mitochondrial lipid oxidation–related genes (carnitine palmitoyltransferase 1β; aconitase 2; and cytochrome *C* oxidase subunit 4 isoform 1) were also activated by Nogo deficiency in HFD-fed mouse skeletal muscle (Fig. 5, *K* and *L*). In addition, Nogo deficiency increased p-AMPKα, PPARα, and AdipoR1 expression in the tissue (Figs. 5*M* and S3, *E* and *F*). HFD feeding increased protein kinase C ε, an inhibitor of insulin signaling, which was substantially blocked by Nogo deficiency (Fig. 5*M*). Therefore, Nogo deficiency also ameliorates HFD-induced lipid accumulation and insulin resistance in mouse skeletal muscle.

### Nogo deficiency attenuates systemic inflammation

The effect of Nogo deficiency on systemic inflammation was determined by a protein array assay (Fig. 6*A*). HFD feeding increased levels of various proinflammatory cytokines in WT mice serum. However, Nogo deficiency substantially blocked HFD-induced expression of these molecules (Figs. 6*A* and S7).

Crown-like structure, a histological hallmark of obesity-associated adipose tissue inflammation, is composed of macrophages surrounding adipocytes. Figure 6*B* shows that Nogo deficiency reduced the number of crown-like structure in eWAT. HFD-activated infiltration of macrophages into liver, iBAT, and islet was also significantly decreased by Nogo deficiency (Fig. 6, *C–E*). Moreover, the percentages of anti-inflammatory M2 macrophages in eWAT and iBAT were increased in HFD-fed Nogo$^{-/-}$ mice, associated with reduced proinflammatory M1 macrophages (Fig. 6, *F–I*). These results suggest that Nogo deficiency decreases expression of proinflammatory cytokines, prevents macrophages from being recruited into metabolic organs, and drives polarization of macrophages into M2 phenotype.

### Nogo deficiency reduces NF-κB p65 expression by enhancing its degradation

In addition to be a critical regulator of inflammatory cytokine expression, NF-κB also induces macrophage infiltration into tissues and M1 type differentiation (26). Our results demonstrate that Nogo deficiency not only potently blocked HFD-activated expression of inflammatory cytokines, particularly the molecules regulated by NF-κB (CD40, CD178 [FAS ligand], granulocyte colony-stimulating factor, interferon-γ, IL-1, IL-12, IL-17, and macrophage inflammatory protein 3α/β [C–C motif chemokine ligand 20 or 19]) (Fig. 6*A* and S7) but

UCP-1 immunohistochemical staining with quantitation of MD (*N* and *O*). Expression of Ucp-1 in sc-WAT; Ucp-1, Prdm16, and Dio2 mRNA in iBAT were determined by qRT–PCR (n = 5; *K* and *M*). $^{\&}p < 0.05$, $^{\&\&}p < 0.01$, $^{\&\&\&}p < 0.001$ *versus* control mice. Atgl, adipose TG lipase; Cidea, cell death–inducing DNA fragmentation factor-alpha–like effector α; Cox5b, cytochrome C oxidase subunit 5b; Cox8b, cytochrome C oxidase subunit 8b; Cpt-1β, carnitine palmitoyltransferase 1β; Dio2, deiodonase 2; eWAT, epididymal white adipose tissue; HFD, high-fat diet; Hsl, hormone-sensitive lipase; iBAT, interscapular brown adipose tissue; NC, normal chow; Ndufb2, NADH:ubiquinone oxidoreductase subunit b2; Nogo, reticulon-4; Prdm16, PR domain containing 16; qRT, quantitative RT; sc-WAT, subcutaneous white adipose tissue; Tbx-1, T-box transcription factor 1; TG, triglyceride; UCP-1, uncoupling protein-1.

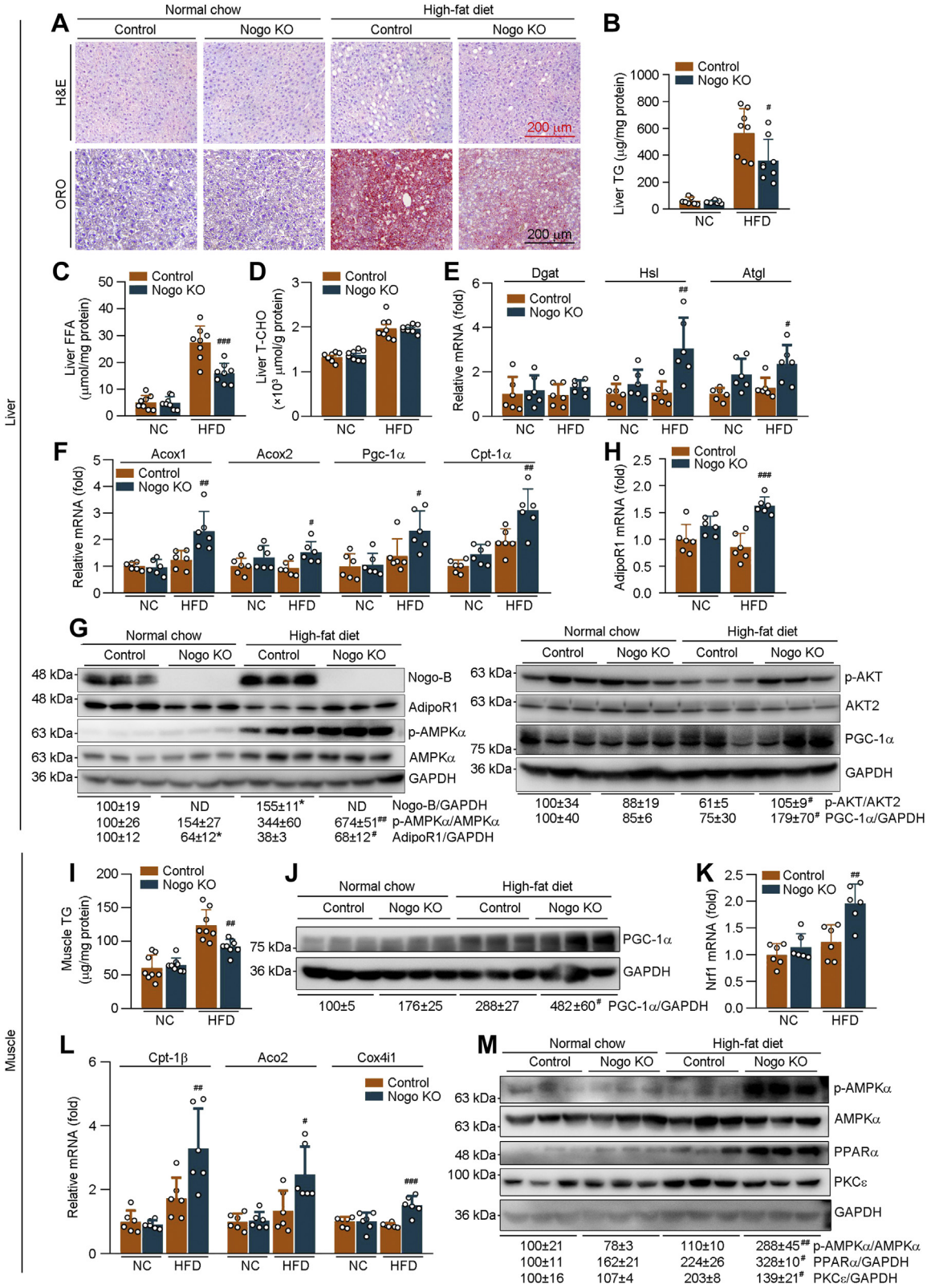


**Figure 5. Nogo deficiency inhibits HFD-induced lipid accumulation in tissues by enhancing lipid oxidation and energy metabolism.** The following assays were conducted on liver or skeletal muscle samples collected from mice used in Figure 2. *A*, H&E and Oil red O staining was conducted on the liver sections. Hepatic TG (*B*), FFA (*C*), and T-CHO (*D*) levels were determined using the corresponding assay kits (n = 8). Expression of TG synthesis/hydrolysis-related genes (Dgat, Hsl, and Atgl; *E*), fatty acid oxidation–related genes (Acox1, Acox2, Pgc-1α, and Cpt-1α; *F*), and AdipoR1 (*H*) in the liver was determined by qRT–PCR (n = 6). *G*, protein expression of Nogo-B, AdipoR1, p-AMPKα, AMPKα; and p-AKT, AKT2, and PGC-1α in the liver was determined by Western blot with quantitative analysis of band density (n = 3). *I*, skeletal muscle TG content was determined using the TG assay kit (n = 8). *J* and *M*, protein expression of PGC-1α; p-AMPKα, AMPKα, PPARα, and PKCε were determined by Western blot with quantitative analysis of band density (n = 3). *K* and *L*, expression of Nrf1; Cpt-1β, Aco2, and Cox4i1 mRNA was determined by qRT–PCR (n = 6). *$p < 0.05$ *versus* control NC-fed mice; #$p < 0.05$, ##$p < 0.01$, ###$p < 0.001$ *versus* control

also reduced HFD-induced macrophage infiltration and M1 polarization (Fig. 6, *B*–*I*). These data imply that NF-κB may play an important role in Nogo deficiency–inhibited inflammation and obesity.

NF-κB p65 is the main subunit of NF-κB protein. As shown in Figure 7, *A* and *B*, lack of Nogo expression not only reduced the basal level of NF-κB p65 but also potentially blocked HFD-activated NF-κB p65 protein expression in mouse liver, WAT, skeletal muscle, iBAT, pancreas, and macrophages in eWAT. Associated with changes in NF-κB p65 protein expression, we determined that Nogo deficiency reduced nuclear NF-κB p65 protein levels in mouse liver (Fig. 7*C*). Consistent with reduced NF-κB p65 activation, HFD-activated mRNA expression of inflammation cytokines (Il-1β, tumor necrosis factor alpha [Tnf-α], and Il-6) and macrophage chemokine (monocyte chemoattractant protein 1) was decreased in Nogo$^{-/-}$ mice in HFD condition (Figs. 7*D* and S8*A*). To further determine the effect of NF-κB p65 on Nogo deficiency–inhibited inflammation cytokine expression and macrophage infiltration, we transfected Ctrl (Ctrl-Cas9) and Nogo-deficient (Nogo-Cas9) HepG2 cells with NF-κB p65 expression vector, followed by treatment with palmitate (mimic high-fat environment). Consistent with the *in vivo* results, Nogo deficiency blocked palmitate-activated mRNA expression of IL-1β, IL-6, and monocyte chemoattractant protein 1 (Fig. 7*E*). However, these inhibitory effects of Nogo deficiency were abolished by NF-κB p65 overexpression (Fig. 7*E*). Taken together, the amelioration of Nogo deficiency on obesity-induced inflammation and macrophage infiltration is dependent on NF-κB p65 inactivation.

IκB can bind to NF-κB and trap it in the cytoplasm. To investigate the underlying mechanisms by which reduced Nogo inactivates NF-κB, we detected IκB and NF-κB p65 protein expression in Ctrl and Nogo-deficient peritoneal macrophages. As shown in Fig. S8*C*, Nogo deficiency significantly decreased total NF-κB p65 but not IκB levels, indicating that Nogo may regulate NF-κB p65 nuclear translocation by affecting its total protein expression rather than IκB. The results in Figure 8*A* showed that NF-κB p65 was increased in 293T cells by high-expressing Nogo-B (C2-Nogo-B) and reduced in Nogo-deficient HepG2 cells (Nogo-Cas9), further confirming that Nogo can influence total NF-κB p65 protein level. Interestingly, neither Nogo high expression nor deficiency had effect on NF-κB p65 mRNA expression (Figs. 8*B* and S8*D*), suggesting that regulation of NF-κB p65 protein expression by Nogo is completed at the post-transcriptional level. To determine if Nogo can regulate NF-κB p65 protein stability, we treated HepG2 cells with cycloheximide, a potent inhibitor of cellular protein biosynthesis, and found that NF-κB p65 protein degradation was increased in Nogo-deficient HepG2 cells (Fig. 8*C*), indicating that Nogo deficiency reduces NF-κB p65 protein stability or enhances its degradation, which can be completed by activating proteasome and/or lysosome. To further verify the role of proteasome or lysosome in Nogo deficiency–enhanced NF-κB p65 protein degradation, we treated cells with a proteasome inhibitor (MG132) or a lysosome inhibitor ($NH_4Cl$) for different time and determined changes of NF-κB p65 protein. Compared with Ctrl cells, high-expressing Nogo-B did not further increase MG132-increased NF-κB p65 protein levels, indicating Nogo deficiency does not activate proteasome (Fig. 8*D*). Meanwhile, $NH_4Cl$ treatment antagonized Nogo deficiency–enhanced NF-κB p65 protein degradation (Fig. 8*E*), suggesting that Nogo deficiency-activated lysosome is blocked. Therefore, Nogo deficiency–enhanced NF-κB p65 protein degradation is mainly completed by activating lysosome pathway.

### *Nogo siRNA ameliorates obesity in mice*

To determine if inhibited Nogo can reduce obesity and associated metabolic disorders, we initially induced obesity in C57BL/6J mice by 25 weeks of HFD feeding and then injected the obese mice Ctrl siRNA (si-scramble) or Nogo siRNA (si-Nogo) five times (once every 3 days). Compared with Ctrl siRNA, Nogo siRNA constantly reduced mouse bodyweight but increased body temperature (Fig. 9, *A* and *B*). Both liver weight and TG levels were reduced by Nogo siRNA (Fig. 9, *C* and *D*). Nogo siRNA also improved HFD-induced hypertriglyceridemia (Fig. 9*D*) without effect on serum cholesterol levels (Table S2) or muscle TG levels (Fig. 9*D*). In addition, mice-injected Nogo siRNA displayed increased iBAT weight (Fig. 9*C*). Associated with reduced lipid accumulation and increased thermogenesis in si-Nogo-injected mice, expression of lipid oxidation–related proteins, such as p-AKT, p-AMPKα, and PGC-1α, in liver and skeletal muscle, was substantially upregulated (Fig. 9, *E* and *F*). Nogo siRNA injection also downregulated NF-κB p65 protein levels (Fig. 9*G*) without affecting its mRNA levels in tissues (Fig. S9*A*). Nuclear translocation of NF-κB p65 was attenuated in si-Nogo-injected mouse liver (Fig. 9*H*), which was associated with decreased mRNA expression of inflammatory cytokines (Il-1β, Tnf-α, and Il-6) and M1 macrophage marker (inducible NO synthase) in liver, skeletal muscle, and WAT, and increased expression of M2 macrophage marker (arginase 1) (Fig. 9*I*). Therefore, these results indicate that inhibited Nogo can ameliorate established obesity by regulating energy metabolism and inflammation.

## Discussion

Obesity is generally associated with dyslipidemia. Interestingly, in this study, we found that human serum Nogo-B levels were positively correlated with BMI and lipid profiles (Fig. 1, *B* and *C*). In mice, Nogo-B expression in tissues, serum, and macrophages was increased by refeeding or increased lipid

HFD-fed mice. Acox, acyl-CoA oxidase; Aco2, aconitase 2; AdipoR1, adiponectin receptor 1; AMPKα, AMP-activated kinase α; Atgl, adipose TG lipase; Cox4i1, cytochrome *C* oxidase subunit 4 isoform 1; Cpt-1α, carnitine palmitoyltransferase 1α; Cpt-1β, carnitine palmitoyltransferase 1β; Dgat, diacylglycerol O-acyltransferase; FFA, free fatty acid; HFD, high-fat diet; Hsl, hormone-sensitive lipase; NC, normal chow; ND, under detectable; Nogo, reticulon-4; Nrf1, nclear respiratory factor 1; p-AMPKα, phosphrylated AMPKα; Pgc-1α, peroxisome proliferator–activated receptor gamma coactivator 1α; PKCε, protein kinase C ε; qRT, quantitative RT; T-CHO, total cholesterol; TG, triglyceride.

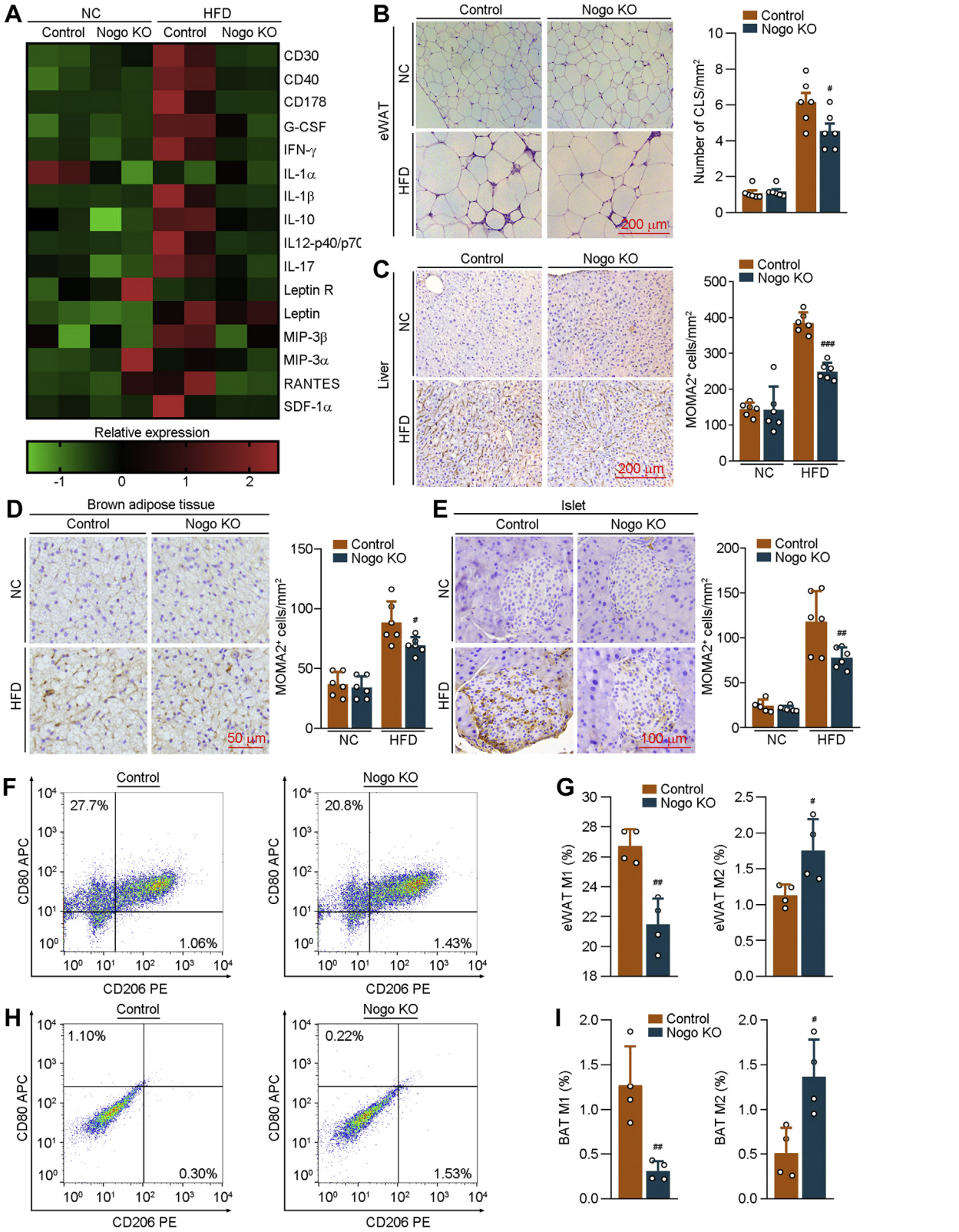


**Figure 6. Nogo deficiency attenuates obesity-induced systemic inflammation.** The following assays were conducted on the serum and tissues collected from mice used in Figure 2. *A*, serum inflammatory cytokines were determined by the mouse cytokine array G3 (RayBiotech) method (n = 2). *B*, H&E staining was conducted on the eWAT sections, and the number of crown-like structure (CLS) was determined. *C–E*, immunohistochemical staining was conducted on the liver, BAT, and islet sections to determine MOMA2 expression with quantitative analysis of MOMA2-positive cells (n = 6). Fractions of M1 and M2 macrophages were determined on eWAT (*F* and *G*) and BAT (*H* and *I*) by FACS (n = 4). $^{\#}p < 0.05$, $^{\#\#}p < 0.01$, $^{\#\#\#}p < 0.001$ *versus* control HFD-fed mice. BAT, brown adipose tissue; eWAT, epididymal white adipose tissue; FACS, fluorescence-activated cell sorting; HFD, high-fat diet; NC, normal chow; Nogo, reticulon-4.

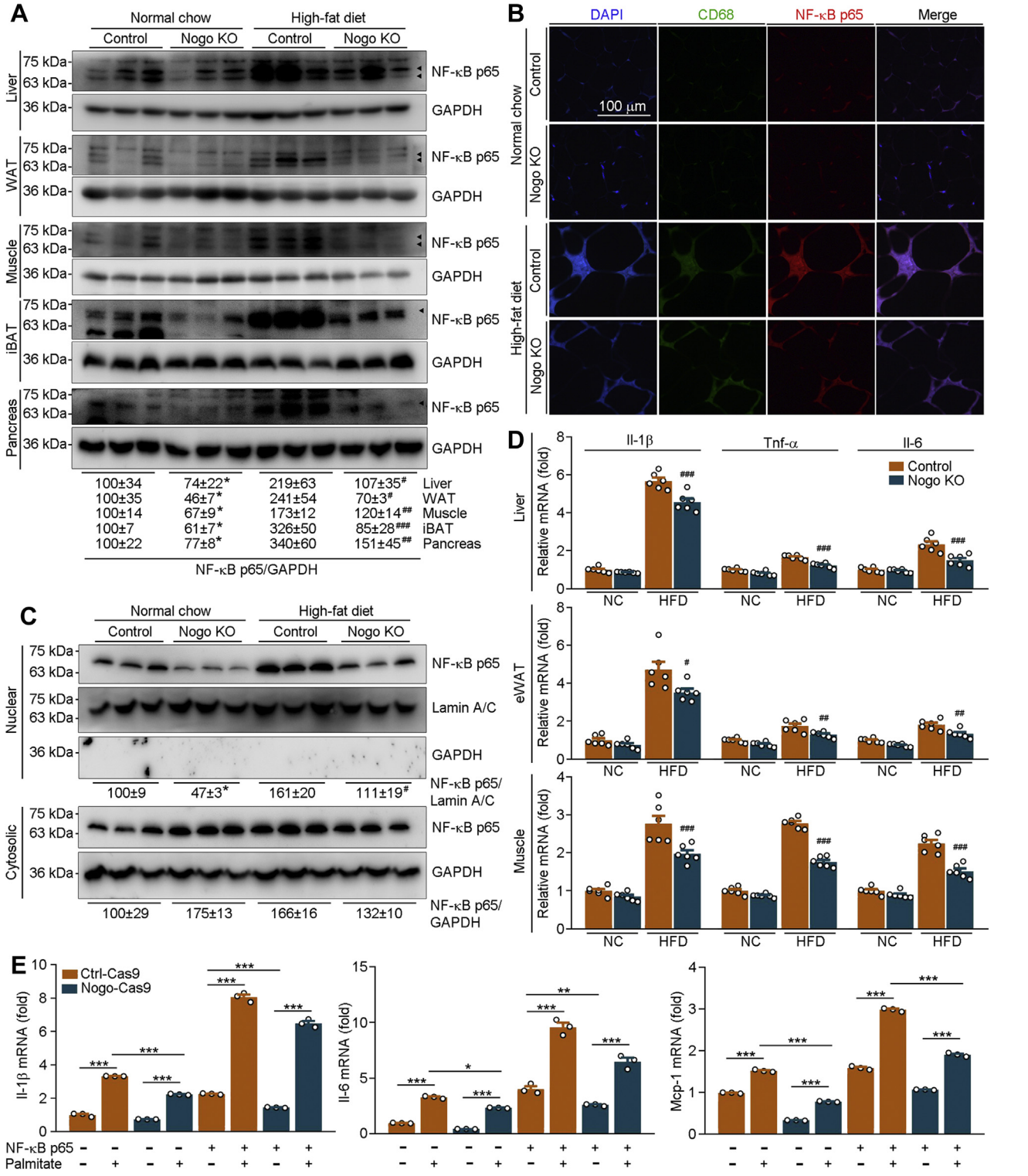


**Figure 7. Nogo deficiency inhibits inflammation by reducing NF-κB p65 protein expression and nuclear translocation.** *A–D*, the following assays were conducted on the liver, eWAT, skeletal muscle, iBAT, and pancreas samples collected from mice used in Figure 2. NF-κB p65 protein expression in liver, skeletal muscle, WAT, iBAT, and pancreas whole extract (*A*), liver nuclear or cytosolic extract (*C*) was determined by Western blot with quantitative analysis of band density (n = 3). Co-immunofluorescent staining was conducted on the eWAT sections with CD68 and NF-κB p65 antibodies (*B*). mRNA expression of Il-1β, Tnf-α, and Il-6 was determined by qRT–PCR (*D*, n = 6). $^{*}p < 0.05$ *versus* control NC-fed mice; $^{\#}p < 0.05$, $^{\#\#}p < 0.01$, $^{\#\#\#}p < 0.001$ *versus* control high-fat diet-fed mice. *E*, Ctrl-Cas9 and Nogo-Cas9 HepG2 cells were transfected with control or NF-κB p65 expression vector for 24 h, followed by 200 μmol/l palmitate treatment for 16 h. mRNA expression of Il-1β, Il-6, and Mcp-1 was determined by qRT–PCR (n = 3). $^{*}p < 0.05$, $^{**}p < 0.01$, and $^{***}p < 0.001$. eWAT, epididymal white adipose tissue; iBAT, interscapular brown adipose tissue; IL, interleukin; Mcp-1, monocyte chemoattractant protein 1; NC, normal chow; Nogo, reticulon-4; qRT, quantitative RT; Tnf, tumor necrosis factor.

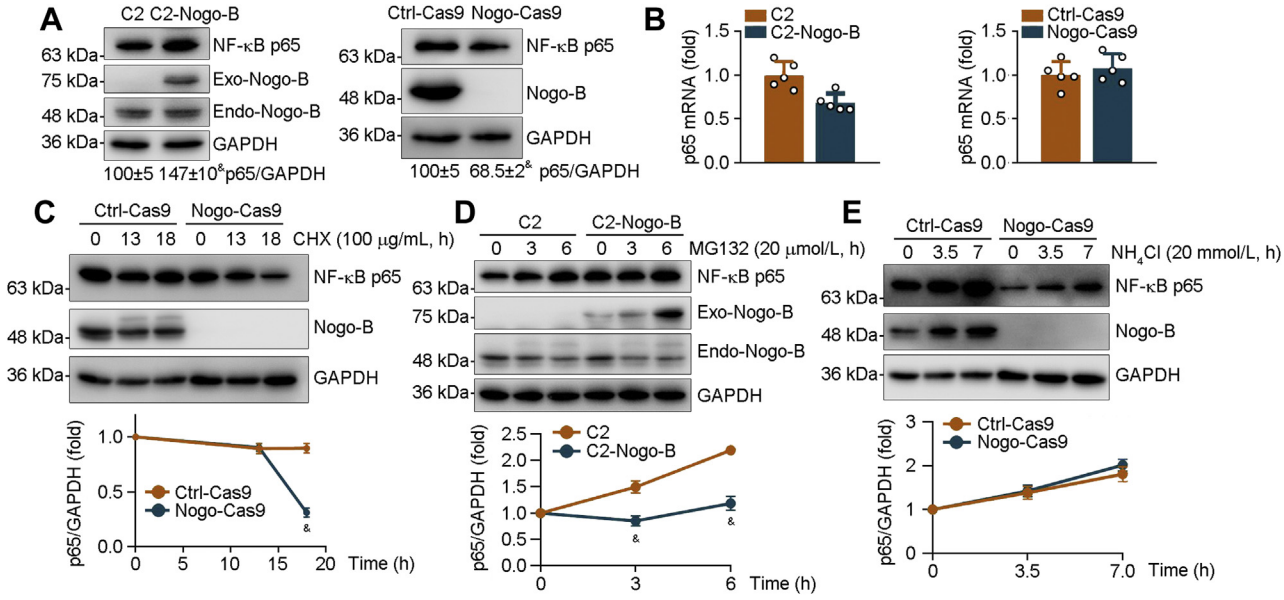


**Figure 8. Nogo deficiency promotes NF-κB p65 degradation**. *A* and *B*, protein expression of Nogo-B and NF-κB p65 was determined in 293T cells transfected with C2 vector or C2-Nogo-B expression vector (*A*, *left panel*) and Ctrl-Cas9 or Nogo-Cas9 HepG2 cells (*A*, *right panel*) by Western blot with quantitative analysis of band density (*A*), and expression of NF-κB p65 mRNA by qRT–PCR (*B*). *C–E*, Ctrl-Cas9, Nogo-Cas9 HepG2 cells (*C* and *E*), or 293T cells transfected with C2 vector or C2-Nogo-B expression vector (*D*) received the following treatment: cycloheximide (CHX, 100 μg/ml, *C*), MG132 (20 μmol/l, *D*), or $NH_4Cl$ (20 mmol/l, *E*) for indicated time. After treatment, total proteins were extracted and used to determine protein expression of NF-κB p65 and Nogo-B by Western blot with quantitative analysis of band density (n = 3). $^{\&}p < 0.05$ *versus* control cells. Nogo, reticulon-4; qRT, quantitative RT.

supplementation in the food (Figs. 1, *D–F*, 5*G*, S1, *C–F*, and S3*D*). Mouse serum Nogo-B levels were also positively correlated with bodyweight and lipid profiles (Fig. S10). Reciprocally, reduced Nogo expression by genetic deletion or siRNA injection potently reduced HFD-induced mouse bodyweight gain (Figs. 2, *A* and *B* and 9*A*), which was associated with reduced liver weight, TG, and FFA levels (Figs. 2*H*, 5, *B* and *C* and 9, *C* and *D*), and circulating TG levels (Table S1 and Fig. 9*D*). Nogo deficiency also reduced serum glucose and enhanced insulin sensitivity (Table S1 and Fig. 2, *F* and *G*). Therefore, our study clearly demonstrates that reduced Nogo expression can ameliorate HFD-induced obesity and related complications.

Obesity is associated with imbalance between energy intake and expenditure. Reducing food intake or nutrient absorption and increasing energy consumption can restrain obesity development. For example, most of the approved drugs for obesity treatment can increase satiety or reduce food absorption (2). In this study, we determined that neither food (normal chow or HFD) intake nor secreted TG and T-CHO in feces was altered by Nogo deficiency (Fig. 2, *C–E*). While, increased oxygen consumption and energy expenditure were observed in HFD-fed Nogo$^{-/-}$ mice (Fig. S2, *A* and *C*). Taken together, inhibition of HFD-induced obesity by Nogo deficiency should be related to enhanced energy metabolism.

Activation of AMPKα increases lipid oxidation and insulin sensitivity, whereas inhibits lipogenesis, thereby reducing obesity development (27). Nogo deficiency activated AMPKα, promoted expression of lipid oxidation–related genes, and attenuated TG deposition in liver and skeletal muscle (Fig. 5). Circulating adiponectin secreted from adipose tissue exists as multimeric complex, such as a lower molecular weight hexamer and/or HMW larger multimeric structures (12–36 multimers). Increased serum HMW adiponectin is primarily associated with enhanced insulin sensitivity, reduced abdominal fat, and high basal lipid oxidation in humans (28). Promotion of adiponectin multimerization protects mice against diet-induced obesity and insulin resistance (29). Our results showed that Nogo deficiency increased circulating HMW adiponectin levels and AdipoR1 protein expression, associated with reduced lipid content in tissues and circulating TG levels, particularly under HFD feeding (Figs. 5 and S3*A*, *E*, and *F*; Table S1), indicating Nogo deficiency activates AMPKα through adiponectin–AdipoR1 axis, which was further confirmed by the *in vitro* study (Fig. S3, *B* and *C*).

Fibroblast growth factor 21 (FGF-21) plays an important role in regulating metabolic homeostasis. Inhibition of Nogo expression reduced high-carbohydrate diet–induced fatty liver, insulin resistance, and other metabolic disorders, which is partially attributed to Nogo deficiency–activated liver FGF-21 expression and circulating FGF-21 (14). In this study, although Nogo deficiency can enhance HFD-increased circulating FGF-21 levels (Fig. S3*G*), it attenuated HFD-induced liver FGF-21 expression (Fig. S3*H*). The different regulation of FGF-21 expression by Nogo deficiency between HFD and high-carbohydrate diet feedings might be related to inactivated carbohydrate response element binding protein and *de novo* lipogenesis under high-carbohydrate diet feeding (14).

The thermogenic activity of BAT and beige cells is also related to obesity development (30). Compared with other cell types, both BAT and beige cells dissipate chemical energy as heat, thereby consuming more lipids to generate the same amount of ATP. Reduced BAT in obese population suggests that promoting the browning of adipose tissue can be a

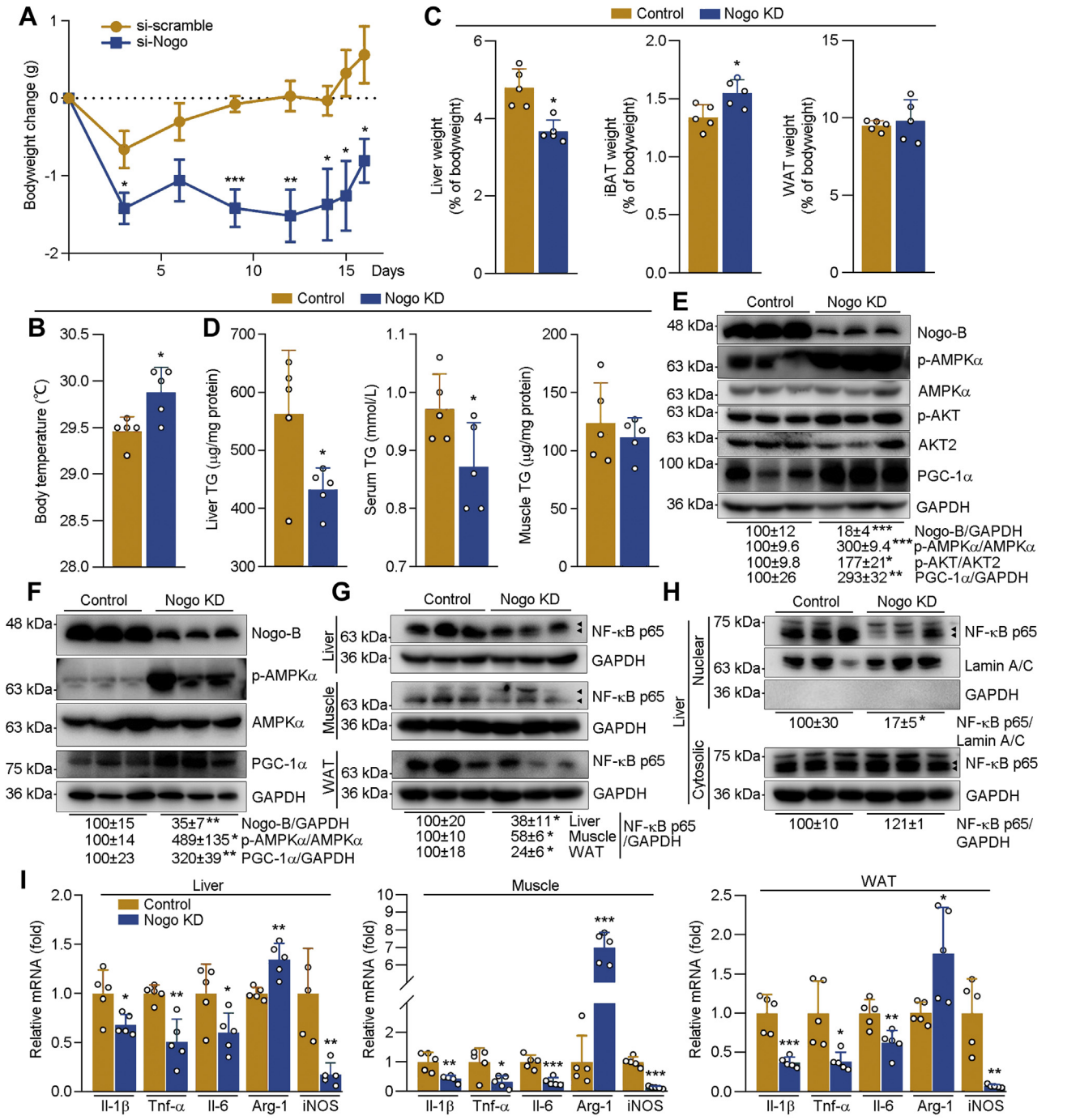


**Figure 9. Nogo siRNA ameliorates HFD-induced bodyweight gain and associated metabolic disorders in mice**. After 25 weeks of HFD feeding, the obese mice (C57BL/6J, male, ~31 weeks old) were divided into two groups (five mice per group) randomly and received tail vein injection of Nogo siRNA (Nogo KD) or scrambled siRNA (control) once every 3 days for five times. *A*, during the treatment, mouse bodyweight was determined at the indicated time points, and the average bodyweight change was calculated. At the end of experiment (3 days after the last siRNA injection), mouse body temperature was measured (*B*). After sacrifice, mouse tissues were collected for the following assays. Mouse liver, iBAT, and WAT were weighed and calculated as percent of tissue weight in bodyweight (*C*); TG levels in liver, serum, and skeletal muscle were determined by the assay kit or the automatic biochemical analyzer (*D*). Protein expression of Nogo-B, p-AMPKα, AMPKα, p-AKT, AKT2, and PGC-1α in liver or skeletal muscle (*E* and *F*), NF-κB p65 in liver, skeletal muscle, and WAT whole extract (*G*), liver nuclear or cytosolic extract (*H*) was determined by Western blot with quantitative analysis of band density; expression of Il-1β, Tnf-α, Il-6, Arg-1, and iNOS mRNA in liver, skeletal muscle, and WAT (*I*) was determined by qRT–PCR. *$p < 0.05$, **$p < 0.01$, ***$p < 0.001$ *versus* control mice, n = 5. AMPKα, AMP-activated kinase α; Arg-1, arginase 1; HFD, high-fat diet; iBAT, interscapular brown adipose tissue; IL, interleukin; iNOS, inducible NO synthase; Nogo, reticulon-4; p-AMPKα, phosphorylated AMPKα; PGC-1α, peroxisome proliferator–activated receptor gamma coactivator 1α; qRT, quantitative RT; TG, triglyceride; Tnf, tumor necrosis factor; WAT, white adipose tissue.

therapeutic strategy for treatment of obesity and metabolic diseases (31, 32). Interestingly, Nogo deficiency significantly increased iBAT weight (Fig. 2*H*) and activated expression of UCP-1 and lipid oxidation–related genes (Fig. 4, *B–F*) after a long-term HFD feeding. Nogo deficiency also increased iBAT weight, multilocular beige cells, and body temperature when mice faced cold exposure (Fig. 4, *H–J*). Similarly, injection of Nogo siRNA to obese mice reduced bodyweight gain and tissue lipid content, associated with increased iBAT weight and body temperature, and activated tissue AMPKα (Fig. 9, *A–F*). These data strongly suggest that promoting adipose tissue browning and thermogenesis are the important anti-obese mechanisms of reduced Nogo.

The metaflammation is a detrimental factor for obesity. Inflammation cytokines, such as IL-1β and TNF-α, generated by infiltrating macrophages, can damage insulin signaling and AMPKα-mediated energy expenditure (33, 34). M2 type macrophages can promote browning of adipose tissue (35). Nogo deficiency substantially reduced HFD-induced inflammatory cytokines in serum, particularly those regulated by NF-κB (Figs. 6*A* and S7). Along with reduced infiltration of monocytes/macrophages into eWAT, liver, iBAT, and islet (Fig. 6, *B–E*), Nogo deficiency also increased M2 macrophages, whereas reduced M1 macrophages in HFD-fed mouse adipose tissues (Fig. 6, *F–I*). Consistently, expression of molecules responsible for macrophage phenotype in mouse tissues was regulated by Nogo siRNA (Fig. 9*I*). These results indicate that reduced Nogo can inactivate NF-κB, the main regulator for inflammation and obesity development (8, 9). Indeed, NF-κB expression and nuclear translocation were clearly attenuated by reduced Nogo (Figs. 7, *A–C*, 9, *G* and *H*, and S8*C*), and the inactivation of NF-κB might be completed by enhanced NF-κB degradation through activation of lysosome pathway (Fig. 8, *C–E*). Therefore, amelioration of HFD-activated inflammation by reduced Nogo is an important mechanism for its anti-obese properties.

Endoplasmic reticulum (ER) stress is also involved in the development of obesity and related diseases. Previous study has shown that overexpression of Nogo can induce ER stress (36). In this article, our results showed that Nogo deficiency ameliorated HFD-induced ER stress–related gene expression (Fig. S11). Adiponectin multimerization is reported to be impaired by ER stress (37). ER stress can also hinder thermogenesis-related gene expression. We supposed that increased HMW adiponectin and enhanced thermogenesis in Nogo$^{-/-}$ HFD-fed mice may be attributed to decreased ER stress. Previous studies have demonstrated that ER stress is associated with biogenesis and mature of lysosome (38, 39). Increased ER stress can impair autophagosome–lysosome fusion, thereby reducing lysosomal degradation of macromolecules, such as protein (38, 40). Thus, we speculated that decreased ER stress may also contribute to enhanced NF-κB p65 lysosome degradation in Nogo-deficient mice as well as the beneficial effects of Nogo deficiency on obesity and related disorders.

Nogo-B receptor (NGBR) is initially identified as a putative receptor for Nogo-B in endothelial cells (41). In this study, we determined that Nogo deficiency had little effect on NGBR protein expression under different conditions (Fig. S12). In addition, our previous article has demonstrated that neither NGBR overexpression nor NGBR inhibition affected Nogo-B expression (42). These results suggest that Nogo-B and NGBR may exert their functions independently.

Taken together, our study demonstrates that reduced Nogo in tissues and circulation can ameliorate HFD-induced obesity and associated metabolic diseases. These functions may, at least in part, be attributed to enhanced lipid oxidation through AMPKα activation, increased thermogenesis by activating UCP-1, and ameliorated inflammatory cytokine expression, macrophage infiltration, and macrophage phenotype switch by inactivating NF-κB pathway. Collectively, our findings provide novel insights into the physiological roles of reduced Nogo in regulating metabolism and inflammation in obesity, indicating that Nogo inhibition can be a therapeutic option for treatment of obesity and its related diseases.

## Experimental procedures

### *Materials*

Sodium palmitate (catalog no.: P9767), cycloheximide (catalog no.: C7698), MG132 (catalog no.: 474787), and AdipoRon (catalog no.: SML0998) were purchased from Sigma–Aldrich. Isoproterenol (catalog no.: HY-B0468) was purchased from Medchemexpress. Rabbit anti-Nogo (catalog no.: NB100-56681) antibody was purchased from Novus Biologicals. Rabbit anti-AMPKα1/2 (catalog no.: sc-25792) and protein kinase C ε (catalog no.: sc-214), mouse anti-fatty acid synthase (catalog no.: sc-55580) and CD68 (catalog no.: sc-20060), and rat anti-MOMA2 (monocyte/macrophage marker; catalog no.: sc-59332) antibodies were purchased from Santa Cruz Biotechnology. Rabbit anti-PPARα (catalog no.: 15540-1-AP), IκB (catalog no.: 10268-1-AP), lamin A/C (catalog no.: 10298-1-AP), SCD (catalog no.: 23393-1-AP), NF-κB p65 (catalog no.: 10745-1-AP) and UCP-1 (catalog no.: 23673-1-AP), mouse anti-PGC-1α (catalog no.: 66369-1-Ig), horseradish peroxidase (HRP)–conjugated GAPDH (catalog no.: HRP-60004), HRP-conjugated α-tubulin (catalog no.: HRP-66031), HRP-conjugated goat anti-rabbit IgG (H + L; catalog no.: SA00001-2) and mouse IgG (H + L; catalog no.: SA00001-1), and goat anti-rabbit IgG (H + L)-rhodamine (catalog no.: SA00007-2) antibodies were purchased from Proteintech Group. Rabbit anti-p-AMPKα (T172; catalog no.: AD0116), AdipoR1 (catalog no.: A16527), and FGF-21 (catalog no.: A3908) antibodies were purchased from ABclonal. Rabbit anti-p-AKT (S473; catalog no.: 4060) and p-F-κB p65 (S536; catalog no.: 3033), and mouse anti-AKT2 (protein kinase B; catalog no.: 5239) antibodies were purchased from Cell Signaling Technology. Rabbit anti-NGBR (catalog no.: ab168351) antibody was purchased from Abcam. Goat anti-mouse IgG (whole molecule)-FITC (catalog no.: F0257) antibody was purchased from Sigma–Aldrich. FITC anti-mouse F4/80 (catalog no.: 123108), PE anti-mouse CD206 (catalog no.: 141706), and APC anti-mouse CD80 (catalog no.: 104714) antibodies were purchased from BioLegend. TG assay kit

(catalog no.: 290-63701) was purchased from Wako Chemicals. T-CHO assay kit (catalog no.: E1026-105) for tissue samples was purchased from Applygen. FFA assay kit (catalog no.: BC0595) was purchased from Solarbio. Human Nogo-B Elisa kit (catalog no.: CSB-EL020572HU) and mouse Nogo-B Elisa kit (catalog no.: CSB-EL020572MO) were purchased from CUSABIO. HMW adiponectin Elisa kit (catalog no.: 47-ADPMS-E01) was purchased from ALPCO. Entranster-*in Vivo* Transfection Regent (catalog no.: 18668-11-1) was purchased from Engreen. Mouse scramble and Nogo siRNA were purchased from GENEWIZ. Human scramble and AdipoR1 siRNA (catalog no.: sc-60123) were purchased from Santa Cruz Biotechnology. Lipofectamine RNAiMAX (catalog no.: 13778100) and Lipofectamine 2000 (catalog no.: 11668019) reagents were purchased from Thermo Fisher Scientific.

### *Plasmid construction*

Human NF-κB p65 expression vector was generated using complementary DNA (cDNA) from HepG2 cells, followed by PCR with forward and reverse primers of 5′-CGGgtac-cATGGACGAACTGTTCCCCCTCATCTT-3′ and 5′-CCGct cgagT TAGGAGCTGATCTGACTCAGCAGG-3′. Letters in lowercase represent the restriction sites of KpnI and XhoI, respectively. The PCR product was digested with KpnI and XhoI and then ligated into a pcDNA3.1(+) plasmid. Human Nogo-B expression vector was constructed as described and named as C2-Nogo-B (14).

### *Cell culture*

HepG2 (human hepatic cell line) or 293T (human embryonic kidney cell line) cells were purchased from American Type Culture Collection and cultured in Dulbecco's modified Eagle's medium containing 10% fetal bovine serum and 50 μg/ml penicillin/streptomycin with or without 2 mmol/l glutamine, respectively.

HepG2 cells lacking Nogo-B expression were established using CRISPR–Cas9 technology as described (13) and named as Nogo-Cas9 cells, whereas the corresponding Ctrl cells were named as Ctrl-Cas9 cells.

### *Collection of human serum samples for biochemical assay*

All experiments with human blood samples were approved by the Clinical Ethics Committee of the First Affiliated Hospital of Anhui Medical University and adhered strictly to the Declaration of Helsinki Principle 2008. Based on the classification on obesity in China (underweight, BMI $< 18.5$ kg/m$^2$, n = 9; normal, $18.5 \le$ BMI $< 24$ kg/m$^2$, n = 12; overweight, $24 \le$ BMI $< 28$ kg/m$^2$, n = 14; obese, BMI $\ge 28$ kg/m$^2$, n = 15), we recruited 50 volunteers at the BMI range of 16.9 to 34.1 kg/m$^2$. All the members were informed and signed the consent at the beginning of recruitment. After collection, blood samples were used to isolate serum by technicians who were blinded to the samples, followed by determination of T-CHO, LDL, and TG levels using an automatic biochemical analyzer (model #3100; Hitachi High-Technologies Corporation). Serum Nogo-B levels were detected using a human Nogo-B Elisa kit.

### *Animals and* in vivo *studies*

All animal experiments were granted by the Ethics Committee (no. HFUT-NKU20190215001C) and conformed to the Guide for the Care and Use of Laboratory Animals published by the National Institutes of Health (publications no.: 8023; revised 1978). C57BL/6J and Nogo-deficient (Nogo KO or Nogo$^{-/-}$, C57BL/6J background) mice originally obtained from Nanjing Biomedical Research Institute of Nanjing University. Nogo$^{-/-}$ mice used in this study were generated using CRISPR–Cas9 system as described (13). The mice were housed in SPF units of the Animal Center at Nankai University (with a 12 h light cycle from 8 AM to 8 PM, 23 ± 1 °C, 60 to 70% humidity) with free access to normal chow and water. Up to five mice were kept per ventilated cage with corn cob bedding material. Mice were allowed to acclimatize to the housing environment for at least 7 days before experiments.

For the fasting experiment, male C57BL/6J mice (∼7 week old) were deprived of normal chow for 24 h. For refeeding experiment, mice were fasted for 24 h and then refed normal chow for 12 h. For a short-term HFD (35% fat containing 60% kcal; catalog no.: D12492; Research Diets) or a high-cholesterol diet (21% fat plus 0.5% cholesterol) feeding, male C57BL/6J mice (∼7 week old) were divided into three groups and fed normal chow, HFD, or high-cholesterol diet for 1 week.

For the long-term HFD feeding experiment, male Nogo$^{-/-}$ mice (∼6 week old) and their age-matched littermate Ctrl (WT, ∼6 week old) mice were divided into two groups randomly. Mice in Ctrl groups were fed normal chow, and in HFD groups were fed HFD for 14 weeks. During the experiment, mouse bodyweight was detected weekly. At the ninth week of experiment, the food intake was determined, and mouse feces was collected. At the 12th week of experiment, the glucose tolerance test was performed. The mice were fasted for 12 h before i.p. injection of D-glucose (2 g/kg bodyweight). Tail vein blood glucose levels were determined before or at the time point of 20, 30, 60, 90, or 120 min after glucose injection using a glucometer. At the 13th week of experiment, the insulin tolerance test was conducted. The mice were fasted for 6 h before i.p. injection of insulin (1 U/kg bodyweight), and tail vein blood glucose levels were determined before or at the time point of 15, 30, 60, 90, or 120 min after insulin injection.

For the cold adaptation experiment, male Nogo$^{-/-}$ mice (∼10 week old) and WT mice (∼10 week old) were housed in 24 h cycles of 12 h at 4 °C and 12 h at room temperature. During the experiment, mice were free to access drinking water and normal chow. The experiment was lasted for 1 week. Mouse body temperature was detected using an electronic thermometer.

For Nogo knockdown experiment, male C57BL/6J mice (∼6 week old) were fed HFD for 25 weeks, then divided into two groups randomly, and received tail vein injection of Nogo siRNA or scrambled siRNA (sequences were listed in Table S3; 40 μg per mouse) once every 3 days for five times. According to the manufacturer's instructions, Nogo siRNA or scrambled

siRNA was dissolved in 0.9% saline solution. Entranster-*in Vivo* Transfection Reagent was premixed with 1.8% saline solution at 1:1 (v:v). The siRNA solution and premixed transfection reagent solution were mixed for 15 min at room temperature and then used for mice injection. During the experiment, mouse bodyweight was determined.

At the end of experiment, all mice were anesthetized and euthanized in a $CO_2$ chamber, followed by collection of blood and tissue samples. Serum was prepared from blood and used to determine alkaline phosphatase, aspartate transaminase, alanine aminotransferase, T-CHO, high-density lipoprotein cholesterol, LDL, and TG using an automatic biochemical analyzer. Serum FFA, Nogo-B, and FGF-21 levels were determined using the corresponding assay kits.

### Fluorescence-activated cell sorting

SVFs from the eWAT and iBAT were prepared as described with minor modifications (43). Briefly, the fresh tissue was minced into small pieces and then digested in a dissociation buffer (10 mg/ml bovine serum albumin, 2 mmol/l glucose, and 4 mg/ml collagenase type II in PBS) under slow continuous rotation (200 rpm) for 30 min at 37 °C. After digestion, the mixture was filtered through a 100 μm filter and then centrifuged for 8 min at 500 *g*. SVF cells were resuspended with red blood cell lysis buffer for 1 min and then centrifuged for 8 min at 500 *g* after addition of PBS. SVF cells were then incubated with FITC anti-mouse F4/80, APC anti-mouse CD80, and PE anti-mouse CD206 antibodies for 15 min at 4 °C in dark, followed by addition of PBS to wash away antibodies. After centrifuged for 8 min at 500 *g*, the PBS-resuspended cells were subjected to flow cytometry analysis using a FACS Calibur (fluorescence-activated cell sorting; Calibur BD Bioscience). Data were analyzed with the FlowJo software (version 10, BD Bioscience).

### Determination of protein expression by Western blot

Cells or mouse tissues were lysed or homogenized in the lysis buffer to extract total proteins. Nuclear proteins were isolated from fresh mouse liver samples using the nuclear extraction kit (Solarbio). The cellular lysates or tissue homogenates were centrifuged and transferred into new tubes. The protein sample was separated by SDS-PAGE and transferred to a nitrocellulose membrane (PALL). The membrane was blocked with 5% fat-free milk in PBS for 1 h at room temperature, followed by incubation with primary antibody in PBS containing 1% bovine serum albumin overnight at 4 °C. Membrane was washed for 3 × 10 min with PBS containing 0.05% Tween-20, then incubated with appropriate HRP-conjugated secondary antibody in PBS containing 1% fat-free milk for 2 h at room temperature. After washed for 3 × 10 min with PBS containing 0.05% Tween-20, the membrane was incubated in the mixture of Western blotting chemiluminescence reagents 1 and 2 (Millipore) followed by scanning with Clinx ChemiCapture (CLINX).

### Quantitative real-time PCR

Total RNA was isolated from cells or tissue samples using TRIzol reagent (Invitrogen). cDNA was synthesized with a reverse transcription kit (New England Biolabs). Gene expression was determined by quantitative real-time–PCR using SYBR Green PCR reagents (Bio-Rad) and primers with sequences listed in Table S4. The mRNA levels were normalized by Gapdh mRNA in the corresponding samples (44).

### Determination of tissue TG, T-CHO, and FFA levels

To determine TG content, ∼30 mg tissue or 80 mg feces was homogenized in 1 ml PBS. About 900 μl of homogenate was used to extract total lipids for TG determination with the TG assay kit, and the rest of the homogenate was used to determine protein content for normalization of TG levels. TG level was expressed as microgram/milligram protein. T-CHO and FFA levels were measured with cholesterol or FFA assay kit according to the corresponding instruction, respectively.

### H&E, Sirius red, Oil red O, immunohistochemical, and immunofluorescent staining

After collection, fresh tissues were fixed in 4% paraformaldehyde at 4 °C overnight, dehydrated using graded ethanol or 30% sucrose solutions, and embedded in paraffin or optimum cutting temperature compound, respectively. Then the embedded tissues were cut into sections of 5 μm for further staining. Before staining, the 5 μm paraffin sections were deparaffinized in xylene and hydrated using graded ethanol solutions. To conduct histologic analysis, H&E or Sirius red staining was conducted on the tissue sections. The paraffin sections were also used to conduct immunohistochemical or immunofluorescent staining to determine MOMA2, UCP-1, CD68, and Nogo protein expression (14). To determine lipid content in the liver, the 5 μm frozen liver sections were incubated in PBS solution for 15 min and then conducted Oil red O staining (14). All images were captured with a Leica microscope. The mean density of images was quantified by the segmentation color-threshold analysis using Photoshop CS6 and normalized by the value of Ctrl mice. The adipocyte size and Sirius red staining were quantified using ImageJ software (National Institutes of Health).

### Statistical analysis

Data were presented as mean ± SD, and all experiments were repeated at least three times independently. At first, all the data were tested for the normal distribution analysis with Graphpad Prism software (version 8; GraphPad Software, Inc). The data followed normal distribution were then analyzed by one-way or two-way ANOVA or unpaired *t* test (two-tailed). Correlation coefficient was calculated using Pearson correlation test, and two-tailed *p* value was calculated. Significant values were considered if $p < 0.05$ ($n \geq 3$).

## Data availability

All data presented are contained within the main article and supporting information.

*Supporting information*—This article contains supporting information.

*Author contributions*—Y. D. and X. Y. conceptualization; Y. C., K. F., and X. L. formal analysis; X. W., S. Z., and Y. C. investigation; X. W. writing–original draft; J. H., Y. I., Y. D., and X. Y. writing–review & editing; X. W., Y. Y., and D. Z. visualization

*Funding and additional information*—This work was supported by the National Natural Science Foundation of China grants 81973316 (to J. H.) and 82173807 (to Y. D.); the China Postdoctoral Science Foundation grant 2020M681914 (to X. Y.); and Tianjin Municipal Science and Technology Commission of China grant 20JCZDJC00710 and the Fundamental Research Funds for the Central Universities (Nankai University) (grant no.: 63211045 to J. H.).

*Conflict of interest*—The authors declare that they have no conflicts of interest with the contents of this article.

*Abbreviations*—The abbreviations used are: AdipoR1, adiponectin receptor 1; AMPKα, AMP-activated kinase α; BMI, body mass index; cDNA, complementary DNA; Ctrl, control; ER, endoplasmic reticulum; eWAT, epididymal white adipose tissue; FFA, free fatty acid; FGF-21, fibroblast growth factor 21; HFD, high-fat diet; HMW, high–molecular weight; HRP, horseradish peroxidase; iBAT, interscapular brown adipose tissue; IL, interlukin; LDL, low-density lipoprotein cholesterol; NGBR, Nogo-B receptor; Nogo, reticulon-4; p-AKT, phosphorylated AKT; p-AMPKα, phosphorylated AMPKα; Pgc-1α, PPARγ coactivator 1α; PPAR, peroxisome proliferator–activated receptor; Scd1, stearoyl-CoA desaturase-1; sc-WAT, subcutaneous white adipose tissue; SVF, stromal vascular fraction; T-CHO, total cholesterol; TG, triglyceride; TNF-α, tumor necrosis factor alpha; Ucp-1, uncoupling protein-1; Vegf-β, vascular endothelial growth factor β.

## References


1. NCD Risk Factor Collaboration (NCD-RisC) (2016) Trends in adult body-mass index in 200 countries from 1975 to 2014: A pooled analysis of 1698 population-based measurement studies with 19.2 million participants. *Lancet* **387**, 1377–1396
2. Kusminski, C. M., Bickel, P. E., and Scherer, P. E. (2016) Targeting adipose tissue in the treatment of obesity-associated diabetes. *Nat. Rev. Drug Discov.* **15**, 639–660
3. Zhao, H., Shang, Q., Pan, Z., Bai, Y., Li, Z., Zhang, H., Zhang, Q., Guo, C., Zhang, L., and Wang, Q. (2018) Exosomes from adipose-derived stem cells attenuate adipose inflammation and obesity through polarizing M2 macrophages and beiging in white adipose tissue. *Diabetes* **67**, 235–247
4. Fink, L. N., Costford, S. R., Lee, Y. S., Jensen, T. E., Bilan, P. J., Oberbach, A., Bluher, M., Olefsky, J. M., Sams, A., and Klip, A. (2014) Pro-inflammatory macrophages increase in skeletal muscle of high fat-fed mice and correlate with metabolic risk markers in humans. *Obesity (Silver Spring)* **22**, 747–757
5. Ying, W., Lee, Y. S., Dong, Y., Seidman, J. S., Yang, M., Isaac, R., Seo, J. B., Yang, B. H., Wollam, J., Riopel, M., McNelis, J., Glass, C. K., Olefsky, J. M., and Fu, W. (2019) Expansion of islet-resident macrophages leads to inflammation affecting β cell proliferation and function in obesity. *Cell Metab.* **29**, 457–474
6. Hayden, M. S., and Ghosh, S. (2012) NF-κB, the first quarter-century: Remarkable progress and outstanding questions. *Genes Dev.* **26**, 203–234
7. Baker, R. G., Hayden, M. S., and Ghosh, S. (2011) NF-κB, inflammation, and metabolic disease. *Cell Metab.* **13**, 11–22
8. Minegishi, Y., Haramizu, S., Misawa, K., Shimotoyodome, A., Hase, T., and Murase, T. (2015) Deletion of nuclear factor-κB p50 upregulates fatty acid utilization and contributes to an anti-obesity and high-endurance phenotype in mice. *Am. J. Physiol. Endocrinol. Metab.* **309**, E523–E533
9. Ke, B., Zhao, Z., Ye, X., Gao, Z., Manganiello, V., Wu, B., and Ye, J. (2015) Inactivation of NF-κB p65 (RelA) in liver improves insulin sensitivity and inhibits cAMP/PKA pathway. *Diabetes* **64**, 3355–3362
10. Misaki, Y., Miyauchi, R., Mochizuki, K., Takabe, S., Shimada, M., Ichikawa, Y., and Goda, T. (2010) Plasma interleukin-1β concentrations are closely associated with fasting blood glucose levels in healthy and preclinical middle-aged nonoverweight and overweight Japanese men. *Metabolism* **59**, 1465–1471
11. McGillicuddy, F. C., Harford, K. A., Reynolds, C. M., Oliver, E., Claessens, M., Mills, K. H., and Roche, H. M. (2011) Lack of interleukin-1 receptor I (IL-1RI) protects mice from high-fat diet-induced adipose tissue inflammation coincident with improved glucose homeostasis. *Diabetes* **60**, 1688–1698
12. Rissanen, A., Howard, C. P., Botha, J., Thuren, T., and Global, I. (2012) Effect of anti-IL-1β antibody (canakinumab) on insulin secretion rates in impaired glucose tolerance or type 2 diabetes: Results of a randomized, placebo-controlled trial. *Diabetes Obes. Metab.* **14**, 1088–1096
13. Zhang, S., Yu, M., Guo, F., Yang, X., Chen, Y., Ma, C., Li, Q., Wei, Z., Li, X., Wang, H., Hu, H., Zhang, Y., Kong, D., Miao, Q. R., Hu, W., *et al.* (2020) Rosiglitazone alleviates intrahepatic cholestasis induced by α-naphthylisothiocyanate in mice: The role of circulating 15-deoxy-δ(12, 14)-$PGJ_2$ and Nogo. *Br. J. Pharmacol.* **177**, 1041–1060
14. Zhang, S., Guo, F., Yu, M., Yang, X., Yao, Z., Li, Q., Wei, Z., Feng, K., Zeng, P., Zhao, D., Li, X., Zhu, Y., Miao, Q. R., Iwakiri, Y., Chen, Y., *et al.* (2020) Reduced Nogo expression inhibits diet-induced metabolic disorders by regulating ChREBP and insulin activity. *J. Hepatol.* **73**, 1482–1495
15. Park, J. K., Shao, M., Kim, M. Y., Baik, S. K., Cho, M. Y., Utsumi, T., Satoh, A., Ouyang, X., Chung, C., and Iwakiri, Y. (2017) An endoplasmic reticulum protein, Nogo-B, facilitates alcoholic liver disease through regulation of kupffer cell polarization. *Hepatology* **65**, 1720–1734
16. Yu, J., Fernandez-Hernando, C., Suarez, Y., Schleicher, M., Hao, Z., Wright, P. L., DiLorenzo, A., Kyriakides, T. R., and Sessa, W. C. (2009) Reticulon 4B (Nogo-B) is necessary for macrophage infiltration and tissue repair. *Proc. Natl. Acad. Sci. U. S. A.* **106**, 17511–17516
17. Wang, Y., Mi, J., Shan, X. Y., Wang, Q. J., and Ge, K. Y. (2007) Is China facing an obesity epidemic and the consequences? The trends in obesity and chronic disease in China. *Int. J. Obes. (Lond.)* **31**, 177–188
18. Scheja, L., and Heeren, J. (2019) The endocrine function of adipose tissues in health and cardiometabolic disease. *Nat. Rev. Endocrinol.* **15**, 507–524
19. Okuno, Y., Fukuhara, A., Hashimoto, E., Kobayashi, H., Kobayashi, S., Otsuki, M., and Shimomura, I. (2018) Oxidative stress inhibits healthy adipose expansion through suppression of SREBF1-mediated lipogenic pathway. *Diabetes* **67**, 1113–1127
20. Sun, K., Kusminski, C. M., and Scherer, P. E. (2011) Adipose tissue remodeling and obesity. *J. Clin. Invest.* **121**, 2094–2101
21. Rosen, E. D., and Spiegelman, B. M. (2014) What we talk about when we talk about fat. *Cell* **156**, 20–44
22. Cannon, B., and Nedergaard, J. (2004) Brown adipose tissue: Function and physiological significance. *Physiol. Rev.* **84**, 277–359
23. Yamauchi, T., Kamon, J., Ito, Y., Tsuchida, A., Yokomizo, T., Kita, S., Sugiyama, T., Miyagishi, M., Hara, K., Tsunoda, M., Murakami, K., Ohteki, T., Uchida, S., Takekawa, S., Waki, H., *et al.* (2003) Cloning of adiponectin receptors that mediate antidiabetic metabolic effects. *Diabetes* **423**, 762–769
24. Kalinkovich, A., and Livshits, G. (2017) Sarcopenic obesity or obese sarcopenia: A cross talk between age-associated adipose tissue and skeletal muscle inflammation as a main mechanism of the pathogenesis. *Ageing Res. Rev.* **35**, 200–221
25. Wu, Z., Puigserver, P., Andersson, U., Zhang, C., Adelmant, G., Mootha, V., Troy, A., Cinti, S., Lowell, B., Scarpulla, R. C., and Spiegelman, B. M. (1999) Mechanisms controlling mitochondrial biogenesis and respiration through the thermogenic coactivator PGC-1. *Cell* **98**, 115–124
26. Chen, D., Xie, J., Fiskesund, R., Dong, W., Liang, X., Lv, J., Jin, X., Liu, J., Mo, S., Zhang, T., Cheng, F., Zhou, Y., Zhang, H., Tang, K., Ma, J., *et al.* (2018) Chloroquine modulates antitumor immune response by resetting tumor-associated macrophages toward M1 phenotype. *Nat. Commun.* **9**, 873
27. Garcia, D., Hellberg, K., Chaix, A., Wallace, M., Herzig, S., Badur, M. G., Lin, T., Shokhirev, M. N., Pinto, A. F. M., Ross, D. S., Saghatelian, A.,

Panda, S., Dow, L. E., Metallo, C. M., and Shaw, R. J. (2019) Genetic liver-specific AMPK activation protects against diet-induced obesity and NAFLD. *Cell Rep.* **26**, 192–208.e6
28. Lara-Castro, C., Luo, N., Wallace, P., Klein, R. L., and Garvey, W. T. (2006) Adiponectin multimeric complexes and the metabolic syndrome trait cluster. *Diabetes* **55**, 249–259
29. Liu, M., Xiang, R., Wilk, S., Zhang, N., Sloane, L., Azarnoush, K., Zhou, L., Chen, H., Xiang, G., Walter, C., Austad, S., Musi, N., DeFronzo, R., Asmis, R., Scherer, P., *et al.* (2012) Fat-specific DsbA-L overexpression promotes adiponectin multimerization and protects mice from diet-induced obesity and insulin resistance. *Diabetes* **61**, 2776–2786
30. Brestoff, J. R., Kim, B. S., Saenz, S. A., Stine, R. R., Monticelli, L. A., Sonnenberg, G. F., Thome, J. J., Farber, D. L., Lutfy, K., Seale, P., and Artis, D. (2015) Group 2 innate lymphoid cells promote beiging of white adipose tissue and limit obesity. *Nature* **519**, 242–246
31. Betz, M. J., and Enerback, S. (2018) Targeting thermogenesis in brown fat and muscle to treat obesity and metabolic disease. *Nat. Rev. Endocrinol.* **14**, 77–87
32. Zhou, X., Li, Z., Qi, M., Zhao, P., Duan, Y., Yang, G., and Yuan, L. (2020) Brown adipose tissue-derived exosomes mitigate the metabolic syndrome in high fat diet mice. *Theranostics* **10**, 8197–8210
33. Steinberg, G. R., Michell, B. J., van Denderen, B. J., Watt, M. J., Carey, A. L., Fam, B. C., Andrikopoulos, S., Proietto, J., Gorgun, C. Z., Carling, D., Hotamisligil, G. S., Febbraio, M. A., Kay, T. W., and Kemp, B. E. (2006) Tumor necrosis factor α-induced skeletal muscle insulin resistance involves suppression of AMP-kinase signaling. *Cell Metab.* **4**, 465–474
34. Vandanmagsar, B., Youm, Y. H., Ravussin, A., Galgani, J. E., Stadler, K., Mynatt, R. L., Ravussin, E., Stephens, J. M., and Dixit, V. D. (2011) The NLRP3 inflammasome instigates obesity-induced inflammation and insulin resistance. *Nat. Med.* **17**, 179–188
35. Cereijo, R., Gavalda-Navarro, A., Cairo, M., Quesada-Lopez, T., Villarroya, J., Moron-Ros, S., Sanchez-Infantes, D., Peyrou, M., Iglesias, R., Mampel, T., Turatsinze, J. V., Eizirik, D. L., Giralt, M., and Villarroya, F. (2018) CXCL14, a brown adipokine that mediates brown-fat-to-macrophage communication in thermogenic adaptation. *Cell Metab.* **28**, 750–763
36. Kuang, E., Wan, Q., Li, X., Xu, H., Zou, T., and Qi, Y. (2006) ER stress triggers apoptosis induced by Nogo-B/ASY overexpression. *Exp. Cell Res.* **312**, 1983–1988
37. Liu, M., Chen, H., Wei, L., Hu, D., Dong, K., Jia, W., Dong, L. Q., and Liu, F. (2015) Endoplasmic reticulum (ER) localization is critical for DsbA-L protein to suppress ER stress and adiponectin down-regulation in adipocytes. *J. Biol. Chem.* **290**, 10143–10148
38. Fang, C., Weng, T., Hu, S., Yuan, Z., Xiong, H., Huang, B., Cai, Y., Li, L., and Fu, X. (2021) IFN-γ-induced ER stress impairs autophagy and triggers apoptosis in lung cancer cells. *Oncoimmunology* **10**, 1962591
39. Mahanty, S., Dakappa, S. S., Shariff, R., Patel, S., Swamy, M. M., Majumdar, A., and Setty, S. R. G. (2019) Keratinocyte differentiation promotes ER stress-dependent lysosome biogenesis. *Cell Death Dis.* **10**, 269
40. Guo, W., Zhong, W., Hao, L., Dong, H., Sun, X., Yue, R., Li, T., and Zhou, Z. (2021) Fatty acids inhibit LAMP2-mediated autophagy flux *via* activating ER stress pathway in alcohol-related liver disease. *Cell. Mol. Gastroenterol. Hepatol.* **12**, 1599–1615
41. Miao, R. Q., Gao, Y., Harrison, K. D., Prendergast, J., Acevedo, L. M., Yu, J., Hu, F., Strittmatter, S. M., and Sessa, W. C. (2006) Identification of a receptor necessary for Nogo-B stimulated chemotaxis and morphogenesis of endothelial cells. *Proc. Natl. Acad. Sci. U. S. A.* **103**, 10997–11002
42. Chen, Y., Hu, W., Li, Q., Zhao, S., Zhao, D., Zhang, S., Wei, Z., Yang, X., Chen, Y., Li, X., Liao, C., Han, J., Miao, Q. R., and Duan, Y. (2021) NGBR is required to ameliorate type 2 diabetes in mice by enhancing insulin sensitivity. *J. Biol. Chem.* **296**, 100624
43. Allen, J., Dey, A., Nissly, R., Fraser, J., Yu, S., Balandaram, G., Peters, J., and Hankey-Giblin, P. (2017) Isolation, characterization, and purification of macrophages from tissues affected by obesity-related inflammation. *J. Vis. Exp.* **122**, 55445
44. Yang, X., Zhang, W., Chen, Y., Li, Y., Sun, L., Liu, Y., Liu, M., Yu, M., Li, X., Han, J., and Duan, Y. (2016) Activation of peroxisome proliferator-activated receptor γ (PPAR γ) and CD36 protein expression: The dual pathophysiological roles of progesterone. *J. Biol. Chem.* **291**, 15108–15118